INVESTIGATING THE ROLE OF COMPLEX I LOSS IN THYROID TUMORIGENESIS

APPROVED BY SUPERVISORY COMMITTEE

David McFadden, MD PhD

Benjamin Tu, PhD

Ralph Deberardinis, MD PhD

Glen Liszczak, PhD

Duojia Pan, PhD

DEDICATION

To my family, colleagues, and friends who have supported me through every step of this journey.

INVESTIGATING THE ROLE OF COMPLEX I LOSS IN THYROID TUMORIGENESIS

by

VICKY LI

DISSERTATION / THESIS

Presented to the Faculty of the Graduate School of Biomedical Sciences

The University of Texas Southwestern Medical Center at Dallas

In Partial Fulfillment of the Requirements

For the Degree of

DOCTOR OF PHILOSOPHY

The University of Texas Southwestern Medical Center at Dallas

Dallas, Texas

August, 2024

ACKNOWLEDGMENTS

I would first like to thank my mentor, Dr. David McFadden, for all of his guidance over the years. I came to his lab as a very "green" PhD student who was changing fields and needed to be taught everything from basic molecular biology to mouse work. I wasn't sure what kind of science I wanted to do, but something about David's scientific philosophy resonated with me – I wanted to learn everything David had to teach me about how to ask interesting scientific questions, be rigorous with my science, and communicate science to others. I am incredibly grateful for all of the generosity and patience over the years that he has exhibited. He has started a lab that really makes science both rigorous and fun. I am also beyond indebted to my colleagues in the McFadden lab both past and present. I did not truly appreciate how important a lab environment could be for a PhD before I began my graduate studies. Any successes I have had can be attributed to colleagues who were beyond kind and generous with their time, expertise, and advice. That same sentiment can be extended to the rest of the K3/L3 floor and the UTSW Biochemistry Department at large. It's been a privilege to have become friends with such incredible colleagues. Through all of the challenges I have faced throughout my graduate studies, I am lucky to have had such incredible friends from my graduate, medical school, undergraduate, and high school years who have been so supportive of all of my years of schooling. Not everyone is lucky enough to have best friends and roommates who greet you when you come home from lab at 1 AM with a plate of food on the table. You are my community and my life. Even closer to home, I owe a lot to my boyfriend Stephen, his dog Shorty, and my own dog Dobby. I'm so lucky to have found someone who not only "tolerates" my work but in fact shows so much interest

and support. I've lost track of the number of times I've had to text Stephen to ask him if he could walk Dobby when an experiment was running late. Thank you to my family as well – Mom, Dad, and Kathy, I love you.

INVESTIGATING THE ROLE OF COMPLEX I LOSS IN THYROID TUMORIGENESIS

Publication No. _____

Vicky Li, PhD

The University of Texas Southwestern Medical Center at Dallas, 2024

Supervising Professor: Dr. David G. McFadden, MD PhD

Changes in cellular metabolism are considered one of the hallmarks of cancer. In 1924, Otto Warburg initially posited that defects in cellular respiration drive tumorigenesis after observing that tumor cells often perform aerobic glycolysis in culture. Since then, multiple studies have demonstrated that most tumors actually require intact cellular respiration for proliferation. However, cancers of the colon, kidney, and thyroid are enriched in loss-of-function mutations predicted to negatively impact respiration. A recent study has shown that a cohort of tall cell variant-papillary thyroid cancer (TCV-PTC) tumors demonstrate widespread loss of Complex I of the electron transport chain. TCV-PTC is a clinically aggressive form of papillary thyroid cancer, driven universally by the BRAF V600E activating mutation. I have developed a murine model of Braf-driven thyroid cancer to investigate the role of Complex I loss in both tumor initiation and progression.

TABLE OF CONTENTS

PRIOR PUBLICATIONS

1. Frank AR, **Li V**, Shelton SD, Kim J, Stott GM, Neckers LM, Xie Y, Williams NS, Mishra P, McFadden DG. Mitochondrial-Encoded Complex I Impairment Induces a Targetable Dependency on Aerobic Fermentation in Hürthle Cell Carcinoma of the Thyroid. *Cancer Discov*. 2023 Aug 4;13(8):1884-1903. doi: 10.1158/2159-8290. PMID: 37262072.
2. Povedano JM, **Li V**, Lake KE, Bai X, Rallabandi R, Kim J, Xie Y, De Brabander JK, McFadden DG. TK216 targets microtubules in Ewing sarcoma cells. *Cell Chem Biol*. 2022 Aug 18;29(8):1325-1332.e4. doi: 10.1016/j.chembiol.2022.06.002. PMID: 35803262.

LIST OF FIGURES

LIST OF TABLES

LIST OF APPENDICES

LIST OF DEFINITIONS

G6P – Glucose-6-phosphte

F6P – Fructose-6-phosphate

1,3-BPG – 1,3-bisphosphoglycerate

ETC – Electron transport chain

IMM – Inner mitochondrial membrane

FMN – Flavin mononucleotide

Fe-S – Iron-sulfur cluster

NSCLC – Non-small cell lung cancer

GBM – Glioblastoma multiforme

TCV-PTC – tall cell variant – papillary thyroid cancer

HCTC – Hürthle cell thyroid carcinoma

LDH – Lactate dehydrogenase

PDX – Patient-derived xenograft

SCLC – Small cell lung cancer

MMR – Mismatch repair

SMASh – Small Molecule Assisted Shutoff

AID – Auxin inducible degron

IAA – auxin

5-Ph-IAA – 5-phenyl auxin

TCA – tricarboxylic acid

cPTC – classical papillary thyroid cancer

MAPK – Mitogen associated protein kinase

MAPKK – Mitogen associated protein kinase kinase

MAPKKK - Mitogen associated protein kinase kinase kinase

TBP – *TPOCreER*; $Braf^{CA/+}$; $p53^{FL/FL}$; $Ndufa9^{WT}$

TBPN – *TPOCreER*; $Braf^{CA/+}$; $p53^{FL/FL}$; $Ndufa9^{FL/FL}$

TB – *TPOCreER*; $Braf^{CA/+}$

TBN – *TPOCreER*; $Braf^{CA/+}$; $Ndufa9^{FL/FL}$

CHAPTER ONE

Introduction

Behind the simple term "metabolism" lies a complex network of chemical reactions all with the same common goal: to facilitate the growth of a living organism. The processes that underlie growth require energy to move forward – in cells, the major currency of energy is the molecule ATP.

The cell has two primary methods of generating ATP: glycolysis and cellular respiration. Glycolysis refers to a series of enzymatic reactions in the cytosol that break down 1 molecule of glucose to two molecules of pyruvate, producing 2 molecules of ATP, 2 molecules of H_2O, and 2 molecules of the reducing equivalent NADH in the process. The process of glycolysis can roughly be broken up into two phases: "spending" and "payoff." After glucose is taken up into the cell through the GLUT family of transporters (Joost & Thorens, 2001; Mueckler et al., 1985; Wang et al., 2020), 2 ATP molecules are "spent." Hexokinase utilizes 1 ATP to phosphorylate glucose to generate glucose-6-phosphate (G6P). After G6P is converted into fructose-6-phosphate (F6P) is then phosphorylated by phosphofructokinase. ATP and NADH are produced from ADP and NAD+ respectively in the "payoff" phase. The oxidation of glyceraldehyde-3-phosphate into 1,3-bisphosphoglycerate (1,3-BPG) reduces two NAD+ molecules into NADH. 4 ATP molecules are generated from the series of conversions from 1,3-BPG to pyruvate (Chandel, 2021).

Cellular respiration refers to the process of oxidative phosphorylation that occurs in the mitochondrion through the actions of the electron transport chain. The electron transport chain (ETC) is comprised of five multi-subunit protein complexes, labeled I through V, that

carry out a series of redox reactions to pair a proton-motive force with ATP production.

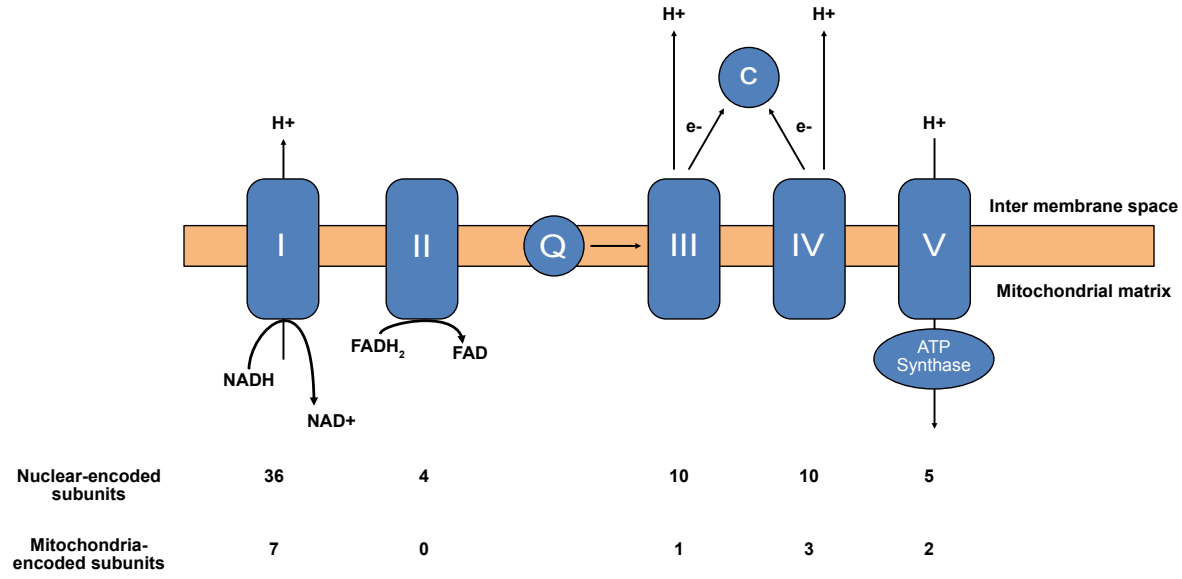

Figure 1. Diagram of the electron transport chain.

Electrons enter the ETC through either Complex I or II. Complex I oxidizes NADH back to NAD+, pairing this redox reaction with the pumping of four protons into the inter-membrane space (IMM) of the mitochondrion. The free electrons released from NAD+ oxidation are transferred first to flavin mononucleotide (FMN), then to the iron-sulfur (Fe-S) clusters in Complex I, and then finally to ubiquinone (Nolfi-Donegan et al., 2020). Ubiquinone is a membrane-bound cofactor which relays the electrons to Complex III. Electrons can also enter the ETC through succinate dehydrogenase, or Complex II (which is also an enzyme in the tricarboxylic acid cycle or TCA cycle). The oxidation of succinate to fumarate releases electrons which are passed through the Fe-S clusters of Complex II to ubiquinone. Ubiquinone relays the electrons released by Complexes I and II to Complex III, or cytochrome c reductase. Complex III pumps four protons into the IMM for every two electrons that it accepts through a process known as the Q cycle (Crofts et al., 2013).

Complex IV, or cytochrome c oxidase, oxidizes Complex III and uses the electrons to reduce oxygen to H_2O. The energy transfer of electrons from Complex III to Complex IV pumps an additional 4 protons into the IMM. The proton gradient generated by the preceding redox reactions provides the energetic basis for the actions of Complex V, ATP synthase. Protons flow down the gradient from the IMM back into the inner mitochondrial space through the "proton corridor" located in ATP synthase. The constant reduction of the "proton corridor" causes the F0 and F1 subunits of ATP synthase to rotate, catalyzing the conversion of ADP to ATP and thus producing energetic equivalents for the cell to survive (Nolfi-Donegan et al., 2020; Zhao et al., 2019). As one turn of glycolysis produces two ATP molecules and one turn of cellular respiration produces 32 ATP molecules, cellular respiration is by far the more efficient of the two ATP production methods.

Mitochondrial proteins are encoded in both the nuclear genome and the mitochondrial genome. The human mitochondrial genome is a 16,569-bp circular piece of DNA that encodes 13 protein subunits of the electron transport chain (Table 1), 2 rRNAs, and 22 tRNAs (Anderson et al., 1981). Unlike the nuclear genome where there are two copies per cell, mitochondria harbor varying copy numbers of the mitochondrial genome. One individual mitochondrion might harbor between 1-15 copies, averaging 5 copies per cell (Satoh & Kuroiwa, 1991). It is also an extremely efficient piece of DNA, with few noncoding bases in between protein coding genes. The majority of mitochondrial proteins are encoded in the nuclear genome; those proteins are subsequently translated in the endoplasmic reticulum and then imported into the mitochondrion through the TIM/TOM protein import complexes (Berthold et al., 1995; Kiebler et al., 1990; Wiedemann et al., 2003).

Gene Name	Product
MT-ATP8	ATP synthase, F0 subunit 8 (complex V)
MT-ATP6	ATP synthase, F0 subunit 6 (complex V)
MT-CO1	Cytochrome c oxidase, subunit 1 (complex IV)
MT-CO2	Cytochrome c oxidase, subunit 2 (complex IV)
MT-CO3	Cytochrome c oxidase, subunit 3 (complex IV)
MT-CYB	Cytochrome b (complex III)
MT-ND1	NADH dehydrogenase, subunit 1 (complex I)
MT-ND2	NADH dehydrogenase, subunit 2 (complex I)
MT-ND3	NADH dehydrogenase, subunit 3 (complex I)
MT-ND4L	NADH dehydrogenase, subunit 4L (complex I)
MT-ND4	NADH dehydrogenase, subunit 4 (complex I)
MT-ND5	NADH dehydrogenase, subunit 5 (complex I)
MT-ND6	NADH dehydrogenase, subunit 6 (complex I)

Table 1. Table of electron transport chain protein subunits encoded by the mitochondrial genome.

ETC dysfunction is pleiomorphic, resulting in a heterogenous array of phenotypes depending on the context. Patients with germline loss-of-function mutations in the *NDUFS4* subunit of Complex I present with a variety of pathologies including but not limited to muscle dystonia, myopathies, or Leigh syndrome, a neurodegenerative disease characterized by hypotonia (low muscle tone) and ataxia (lack of control over movement) (Budde et al., 2003; Petruzzella et al., 2001). *Ndufs4* knockout (KO) mice develop wasting symptoms

similar to Leigh syndrome (Kruse et al., 2008). Mice with cardiac muscle-specific deletion of *Ndufs6*, another Complex I subunit, develop severe cardiomyopathy (Ke et al., 2012). Knockout of polymerase gamma (*Polg*), the mitochondria-specific DNA polymerase, in a murine model results in accelerated mitochondrial DNA mutation accumulation and symptoms of premature aging in mice including kyphosis (hunching), alopecia, and weight loss (Trifunovic et al., 2004).

While a plethora of evidence exists to support the argument that ETC dysfunction is disadvantageous for most cell types, ETC dysfunction is neither universally beneficial nor detrimental to cancer and tumorigenesis. Abnormal metabolism is also one of the earliest known features of cancer. In the early twentieth century, the German physiologist Otto Warburg noted that tumor cells grown in two-dimensional cell culture rapidly acidified cell culture media (Warburg et al., 1927). Working backwards, he determined that this acidification was due to an overproduction of lactate and a direct consequence of these cultured tumor cell lines performing aerobic glycolysis (Warburg et al., 1927). Typically, in oxygen-replete environments, the cell typically relies upon cellular respiration as its primary ATP production method. The term "aerobic glycolysis" therefore refers to a condition where the cell is relying upon glycolysis as its primary ATP production method even in the presence of oxygen which should normally facilitate cellular respiration (Jones & Bianchi, 2015). Warburg also hypothesized that this aerobic glycolysis arose as a result of inherent tumor mitochondrial dysfunction and that an inability to perform cellular respiration could be a tumor driver.

Since Warburg's time, there have been numerous studies demonstrating that the Warburg Hypothesis is not generalizable to most cancer types. Multiple groups have demonstrated that ablation of cellular respiration is an impediment to tumor growth. Infusion of non-small cell lung cancer (NSCLC) patients and glioblastoma multiforme (GBM) patients with radiolabeled glucose reveal that tumor tissue takes up glucose and incorporates it into the TCA cycle at even higher rates than paired adjacent normal tissue, indicating that those tumor tissues are heavily reliant upon cellular respiration as a means of energy production (Hensley et al., 2016; Maher et al., 2012; Weinberg et al., 2010).

Certain cancer types, however, consistently retain DNA mutations that confer loss of cellular respiration. Respiration deficiency is known to occur in both benign and malignant tumors. Benign ETC-deficient tumors include renal oncocytoma, parotid gland oncocytoma, and Hürthle adenomas of the thyroid (Gopal, Calvo, et al., 2018; Joshi et al., 2015; Singh et al., 2023; Tallini, 1998; Yuan et al., 2020). Certain malignant tumor types are also enriched in mutations in mitochondrial DNA-encoded subunits of ETC proteins including thyroid, colorectal, and kidney cancers (Gorelick et al., 2021; Yuan et al., 2020). Our group is interested in two subtypes of thyroid cancer that often harbor ETC deficiencies: Hürthle cell thyroid carcinoma (HCTC) and tall cell variant – papillary thyroid cancer (TCV-PTC). Both tumors have been shown to harbor predicted loss-of-function mutations in mitochondrial DNA-encoded subunits Complex I (Ganly et al., 2018; Gopal, Kubler, et al., 2018; Tsybrovskyy et al., 2022). These examples of true "Warburgian" tumors raise the question of whether Complex I loss – and thereby electron transport chain dysfunction – is merely tolerated in these contexts or, in fact, promotes tumorigenesis.

How are these Complex I null tumors compensating energetically for their metabolic dysfunction? Prior work has been done to characterize how Complex I null cells compensate for their metabolic dysfunction. As the ETC plays an integral in multiple biological functions of the cell including but not limited to ATP production and NAD+ regeneration, the question of how Respiration-incompetent cells have been shown to be auxotrophic for pyruvate (King & Attardi, 1989). Later work has shown that this pyruvate requirement stems from the need to generate aspartate in order to restore NAD+ levels (Birsoy et al., 2015; Sullivan et al., 2015). Cells with deficient Complex III are auxotrophic for both pyruvate and uridine. In addition to the need to generate aspartate, cells lacking Complex III also cannot convert ubiquinol to ubiquinone. The ubiquinol to ubiquinone conversion is necessary for the activity of DHODH, the rate-limiting enzyme in the pyrimidine biosynthesis pathway (King & Attardi, 1989).

In addition, one wonders if these tumors' compensation mechanisms might provide a therapeutically tractable target. Our lab has previously published work demonstrating that HCTC-derived xenograft growth is abrogated after treatment with inhibitors of lactate dehydrogenase (LDH), putting forth lactate fermentation as a potential exploitable liability in HCTC (Frank et al., 2023). Without Complex I's NADH activity, the cell becomes dependent on the NAD+ regenerated in the process of fermenting lactate to pyruvate. Other groups have shown that the treatment of HCTC xenografts with the SLC71AA (cysteine transporter) inhibitor sulfasalazine slows xenograft growth, suggesting that ferroptosis inhibition might be a potential target for HCTC (Gopal et al., 2023). Yet others have published data showing that the mTOR inhibitor rapamycin slows tumor growth in a HCTC

patient-derived xenograft (PDX) implanted inside the renal capsule of NSG mice (Dong et al., 2022). Despite these previous advances, little is known about the mechanisms that explain why Complex I might promote thyroid tumorigenesis. In addition, although much work has been done in HCTC using cell lines and cell line-derived xenografts, no animal model exists for Complex I loss in the setting of thyroid tumorigenesis.

At the beginning of my doctoral work, I developed a novel forward genetics system to improve target identification of small molecules in small cell lung cancer (SCLC). After successfully developing the system, I pivoted to focus my efforts on probing HCTC and TCV-PTC pathogenesis. I performed unbiased nutrient and genetic screens to identify potential vulnerabilities of HCTC. I also characterized a novel murine model of Complex I loss in thyroid tumorigenesis using an autochthonous mouse model generated using disease-relevant mutations.

CHAPTER TWO

Target identification of anti-cancer compounds

2.1 Introduction

As we enter the era of personalized medicine and unprecedented access to massive disease-relevant sequencing datasets, understanding of small molecule mechanism of action is highly valuable for understanding which patients might benefit from certain therapies as well as understanding drug resistance mechanisms.

Both biochemical and genetic methodologies have been utilized to identify small molecule targets. In the 1950s, Leonard Lerman demonstrated that he could improve mushroom tyrosinase purification yield by running mushroom lysate through a solution containing azophenol tyrosinase inhibitors (Lerman, 1953). Subsequently, affinity chromatography has been applied to identifying protein targets of small molecules. Affinity chromatography revealed that the natural product Diazonamide A inhibits spindle assembly by binding ornithine delta-amino transferase (Wang et al., 2007).

Earlier efforts to employ forward genetics to identify small molecule protein targets have relied upon using unbiased gene knockdown to identify genetic modifiers of target efficacy (Parsons et al., 2004). Later, large-scale RNAi gene perturbations in mammalian cells were used to prove that a phenotypic screen for small molecules that target the Rho cytokinesis regulatory pathway were on-target (Castoreno et al., 2010).

Forward genetics tools have continued to diversify. Patients with Lynch syndrome harbor germline mutations in genes that encode for protein components of the DNA mismatch repair (MMR) pathway (Win et al., 2017). The most commonly mutated genes in Lynch syndrome

patients are *PMS2*, *MLH1*, *MSH2*, and *MSH6* (Yurgelun et al., 2017). In patients, deficiency in DNA mismatch repair leads to a higher mutational burden and, subsequently, cancer in multiple organs including the colon. Multiple groups have previously utilized HCT116, a DNA mismatch repair-deficient colorectal cancer cell line, to identify targets of small molecules by raising compound-resistant clones and performing transcriptome sequencing to identify mutations in protein-coding genes that occur in more than one clone (Han et al., 2016; Han et al., 2017; Wacker et al., 2012). HCT116's inherent lack of DNA mismatch repair (MMR) created a cell line that naturally accumulates DNA mutations much more rapidly than other cell lines with intact DNA mismatch repair mechanisms. More recently, our lab demonstrated that engineering constitutive mismatch repair deficiency into mammalian cell lines is a viable strategy for identifying targets of small molecules through unbiased forward genetic screens (Frank et al., 2024; Povedano et al., 2019).

While cell lines harboring constitutive MMR defects have been successfully utilized to identify protein targets of anti-cancer compounds, such systems have limitations. Cell lines with constitutive mismatch repair defects will continue to acquire novel mutations long after compound selection has been completed, leaving researchers to sift through an unwieldy number of mutations in protein-coding genes to identify novel compound targets in an unbiased fashion. Developing an inducible mismatch repair system offers two primary benefits. First, such a system would decrease the final number of candidate mutations by shortening the duration of mismatch repair deficiency. Second, an inducible system offers a clean "mother-daughter" pair to enable accurate calling of mutations that are present in the

parental population versus those that are acquired and selected for while the cells are exposed to the compound of interest.

2.2 Results

One of our lab's primary interests is identifying small molecules that can target small cell lung cancer (SCLC). SCLC disease is a neuroendocrine carcinoma with poor clinical outcome; when the disease is limited at initial diagnosis, median survival time ranges from 15-20 months (Albain et al., 1991; Lassen et al., 1995). Owing to its clinical severity, there is an unmet clinical need for novel SCLC therapeutics. The most common genetic alterations found in SCLC are loss-of-function mutations in tumor suppressor genes such as *P53* and RB1 (Helin et al., 1997; Lassen et al., 1995; Miller et al., 1992; Takahashi et al., 1991). As such, it is difficult to devise targeted therapies for SCLC given that rational design of targeted therapies is best suited for cancers driven by gain-of-function mutations.

Our lab has conducted phenotypic high-throughput chemical screens to identify selective toxins for SCLC. In order to improve our pipeline for identifying targets of small molecule hits from our screen, we decided to engineer our improved forward genetics system into 518T2, a SCLC cell line derived from a lung tumor in a genetically engineered $p53^{FL/FL}$, $p130^{FL/FL}$, $Rb^{FL/FL}$ murine model of SCLC (Schaffer et al., 2010). As earlier mismatch repair (MMR) deficient cells were genetically engineered by knocking out the MMR protein Msh2, we decided to knock in an inducible degron system into the endogenous C-terminal *Msh2* locus.

I set out to genetically engineer a system where DNA mismatch repair was intact at baseline and, upon small molecule-assisted degradation of the Msh2 protein, selectively

induce DNA mismatch repair deficiency. I attempted to target the C-terminal of the Msh2 locus with constructs encoding the necessary components of either the SMASh (Small Molecule Assisted Shutoff) and the AID (Auxin Inducible Degron) conditional protein degradation systems. The SMASh system (Chung et al., 2015) requires knocking in an HCV protease linked to the SMASh degron via an HCV protease cleavage site; the HCV protease will constitutively cleave off the SMASh degron, leaving the target protein intact. Upon the addition of the HCV protease inhibitor danoprevir, the SMASh degron will remain affixed to the protein of interest (POI) and thus targets the POI for degradation. The AID system is a conditional protein system that co-opts components of the ubiquitin-proteasome system that are typically unique to plants. The plant hormone auxin (IAA) recognizes protein degrons and thus acts as a "molecular glue" targeting proteins harboring said degrons for degradation through the SCF/TIR1 F-box E3 ligase complex (Gray et al., 1999; Gray et al., 2001). This system can be re-configured for inducible mammalian protein degradation by knocking in the AID degron into the locus encoding for a POI and introducing the TIR1 F-box protein into the same cell (Nishimura et al., 2009). In the absence of exogenous auxin, the POI will not be degraded. In the presence of exogenous auxin, TIR1/SCF E3 ligase complex will recognize the POI and degrade the POI through the proteasome.

Initial attempts at knocking in either a SMASh or AID degron were not successful, so I decreased homology arm size from 1000 bp to roughly 500 bp and began to screen different constructs as well as antibiotic resistance cassettes. I successfully targeted the 518T2 cell lines using a Msh2-P2A-BSD construct (Figure 2A). After optimizing transfection efficiency, I screened 87 clones. Of the 87 clones, 17 clones had at least 1 knock-in allele by genotyping.

3 clones, B7, C8, and C11, only expressed AID-tagged Msh2 at the protein level as assessed by Western blot (Figure 2B).

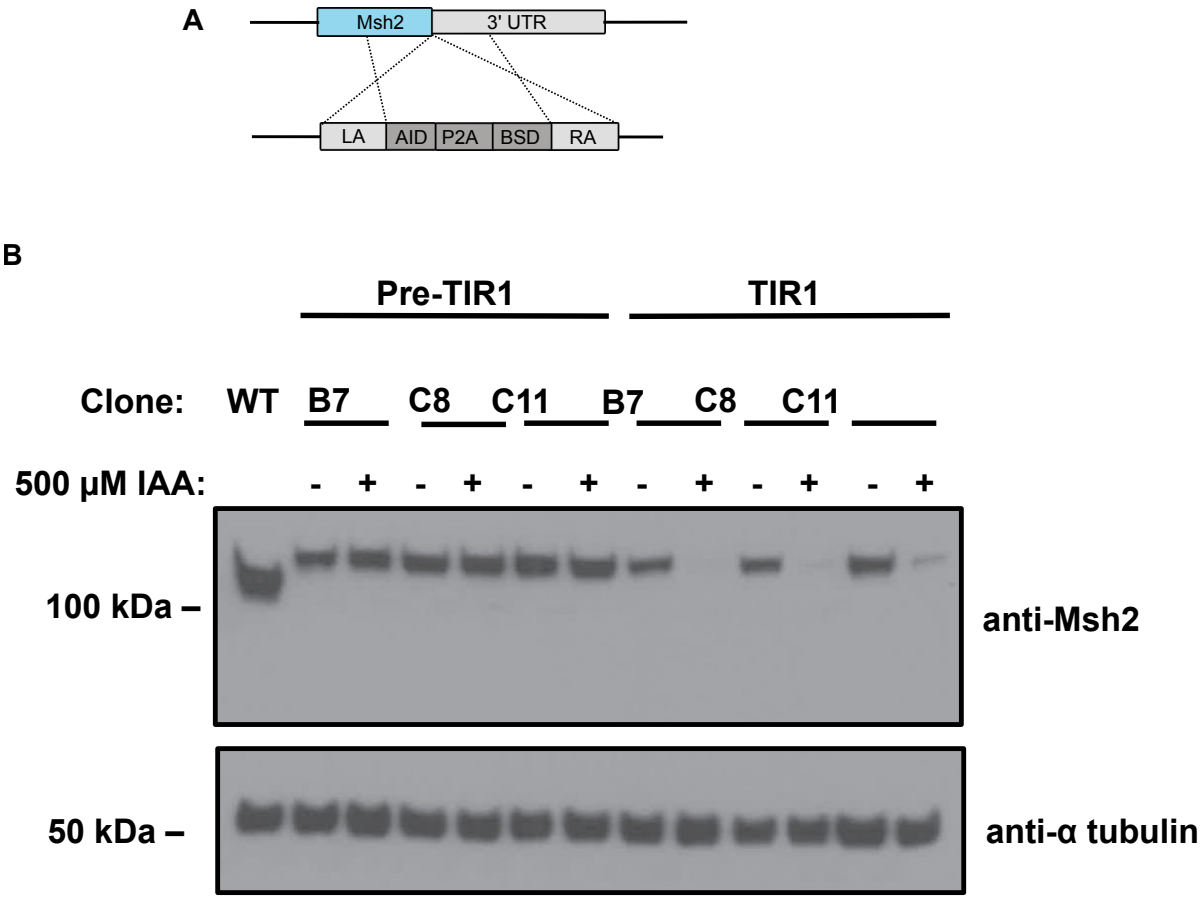

Figure 2. C-terminal targeting of Msh2 locus with AID degron. A) Schematic for AID targeting. B) Western blot validation of three Msh2-AID clones.

All three clones demonstrated low levels of IAA-independent degradation, as their Msh2-AID protein levels were lower once TIR1 was introduced in the absence of IAA (Figure 2B). However, as this appeared to be a very mild phenotype, these clones still appear to be viable candidates for our desired inducible system. I then transduced the three clones with a TIR1-expressing lentivirus to assess TIR-1 dependent degradation. The B7 and C8

clones demonstrated the most efficient Msh2 degradation at 48 hours post-IAA treatment (Figure 2B). All subsequent experiments are performed using the C8 clone.

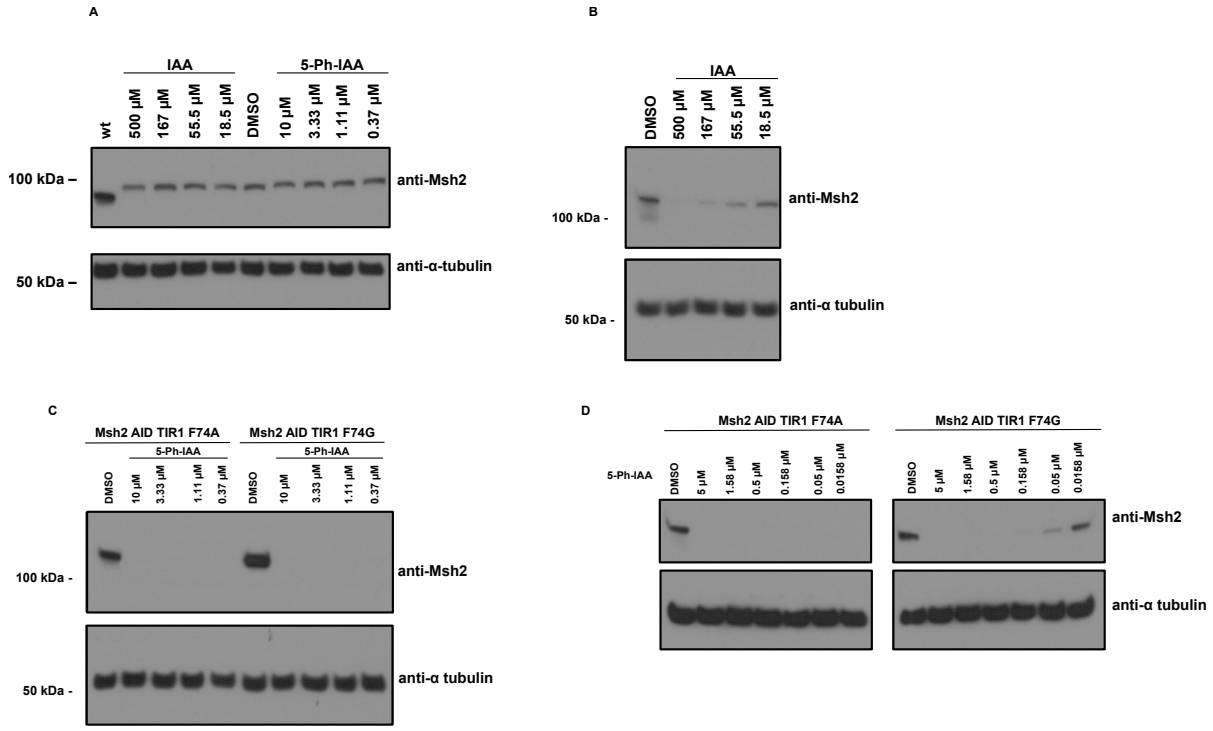

Figure 3. Optimization of AID protein degradation system. A-D) Western blotting of Msh2-AID clone C8. All blots done at 48 hours post-treatment.

After successfully validating the knock-in, I introduced two novel TIR1 mutants that had been shown to recognize the AID* degron with a higher affinity than wildtype TIR1 (Yesbolatova et al., 2020). The novel TIR1 mutants preferentially recognize a modified 5-Phenyl auxin (5-Ph-IAA). The bulkier auxin analog is designed to bind more tightly to the "hole" left in the TIR1 mutants after replacing the bulkier F74 residue with either alanine or glycine. I verified that wildtype TIR1 is unable to recognize 5-Ph-IAA (Figure 3A). After transducing 518T2 with either TIR1 F74A or TIR1 F74G, I validated that both constructs were able to facilitate efficient degradation of Msh2 within 48 hours at nanomolar

concentrations of 5-Ph-IAA (Figure 3C). I also wanted to compare the degradation efficiency of the wildtype TIR1/IAA system with that of the modified F74A/F74G/5-Ph-IAA systems. The wildtype IAA system is unable to fully degrade the Msh2-AID tagged protein at concentrations lower than 500 μM (Figure 3B). The F74A system and F74G system however, require much less 5-Ph-IAA to fully degrade the same Msh2-AID tagged protein. I saw full degradation of Msh2-AID at 48 hours of treatment using as little as 158 nM 5-Ph-IAA with the F74G system and as little as 15.8 nM 5-Ph-IAA with the F74A system (Figure 3C-D). Future experiments with the Msh2-AID inducible degradation system will employ the F74A/5-Ph-IAA system due to its increased efficiency over the wildtype TIR1/IAA system.

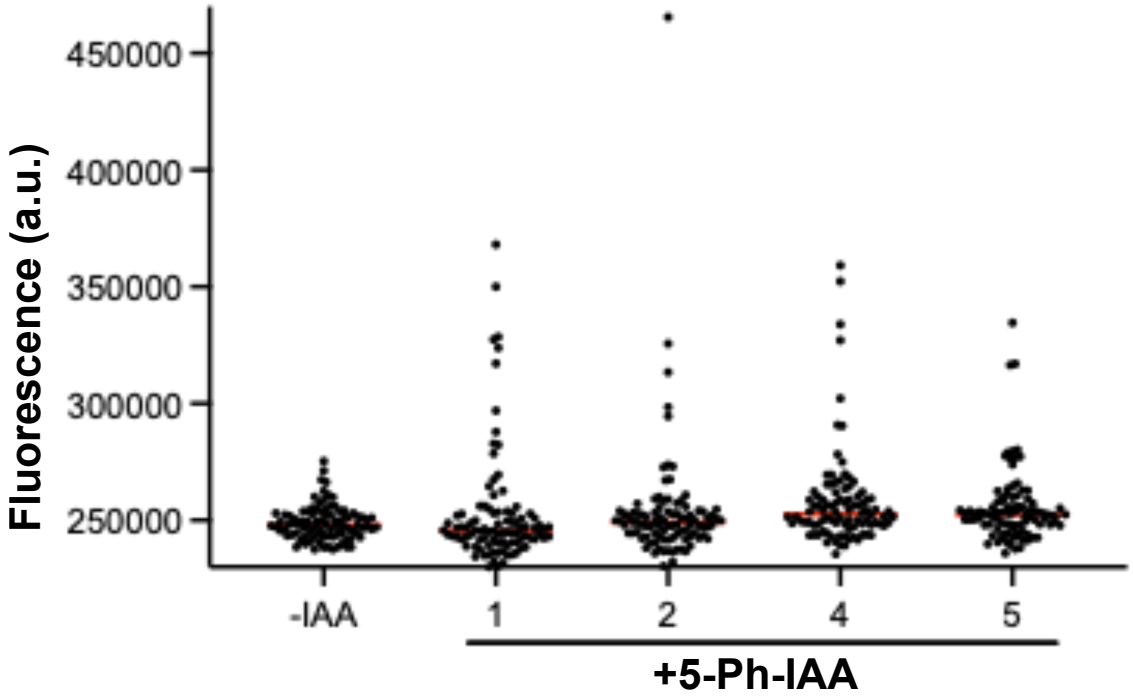

Figure 4. Msh2-AID system is capable of raising putative compound-resistant clones to bortezomib. Alamar blue staining of 518T2 Msh2-AID cells post-incubation with 18 nM bortezomib. Data from Juan Manual Povedano.

Subsequent work by a postdoctoral fellow in my lab, Dr. Juan Manuel Povedano, has demonstrated that the Msh2-AID system is a viable forward genetics system to identify protein targets of small molecules. Dr. Povedano incubated 518T2 Msh2-AID cells with and without 300 nM 5-Ph-IAA for over 3 weeks in the presence of 18 nM bortezomib, a known inhibitor of the proteasome. After incubation, Dr. Povedano stained surviving clones with Alamar blue, a resazurin-based solution that is reduced by the environment of viable cells and fluoresces as a result. Dr. Povedano demonstrated that putative compound-resistant clones emerged from 518T2 Msh2-AID cells that received 5-Ph-IAA while no resistant clones emerged from 518T2 Msh2-AID cells that had not received 5-Ph-IAA (Figure 4).

2.3 Discussion

As outlined above, I have generated a novel system of inducible MMR deficiency in a murine SCLC cell line. We believe that this new inducible system will improve upon the drawbacks of our current system for identifying small molecule targets in SCLC which utilizes a mSCLC cell line with constitutive engineered MMR deficiency. Another group at UT Southwestern has already demonstrated the ability to use a system of inducible mismatch repair deficiency to identify compounds that are cytotoxic to the HCT116 colorectal cancer cell line (Nguyen et al., 2023). Their success combined with promising data generated using our known cell line gives us further confidence that our new system is a viable method of target identification.

Future work on further refining forward genetics-based target identification strategies will primarily focus on more heavily mutagenizing the genomes of cells that are undergoing compound selection. Currently, if selection with a compound of interest is unable to yield

any resistant clones, this failure might either be due (1) to a biological limitation of the system, where the protein target of the compound does not tolerate any mutations that might confer resistant to the compound or (2) a technical limitation of the system, where the cell did not happen to acquire a DNA mutation that would have conferred compound resistance. To address this issue, we plan to increase the mutagenesis rate of our Msh2-AID system by introducing inducible loss of DNA polymerase epsilon, or *PolE*. Previous sequencing studies of pediatric patients with biallelic MMR deficiency (bMMRD) have shown that bMMRD patients with *POLE* loss and MMR deficiency have a drastically higher mutational burden than bMMRD patients with MMR deficiency alone (Shlien et al., 2015).

CHAPTER THREE

Identifying genetic vulnerabilities of Hürthle cell thyroid carcinoma

3.1 Introduction

There are, however, a select few tumor types that appear to be more classically "Warburgian." One such disease is Hürthle cell thyroid carcinoma (HCTC). This disease is primarily diagnosed based on pathology. Upon hematoxylin & eosin (H&E) staining, HCTC is primarily composed of Hürthle cells, enlarged thyroid follicular cells characterized by large, round nuclei and granular eosinophilic cytoplasm. The eosinophilic cytoplasm of the Hürthle cell is caused by mitochondrial accumulation in the cytoplasm (Feldman et al., 1972). This mitochondrial accumulation occurs in a variety of neoplasms termed "oncocytomas" (Gasparre et al., 2011). Oncocytomas can arise in a variety of organs including but not limited to the salivary gland, thyroid, and kidney. While historically considered a subtype of follicular thyroid cancer (FTC), in 2017 HCTC was re-classified in the WHO guidelines as a distinct tumor type that is a cancer type derived from follicular thyroid cells but not a subtype of FTC (Lloyd RV, 2017).

Hürthle cell thyroid carcinoma accounts for roughly 5% of all differentiated thyroid neoplasms (Bhattacharyya, 2003). Although Hürthle cells were first described by the German-Swiss pathologist Max Askanazy in a patient with Graves disease, these cells were named after Karl Hürthle who referred to parafollicular C cells as "Hürthle cells". The first

description of HCTC was published by the German physiologist Theodor Langhans (Langhans, 1907).

Multiple groups have independently documented the association between putative loss-of-function mutations in Complex I and the oncocytic phenotype in thyroid cancer (Bonora et al., 2006; Gasparre et al., 2007; Maximo et al., 2002; Tallini et al., 1994). Our group more recently published a study in which we performed exome sequencing on tumor samples from a cohort of HCTC patients and made two key findings. First, we found that 54% of HCTC patient tumor genomes harbored widespread chromosomal losses that resulted in a "near-haploid" state with key exceptions being chromosomes 5, 7, 12, and 20. Other groups had observed chromosomal abnormalities before (Wada et al., 2002). Second, we confirmed observations from earlier work linking mutations in Complex I to oncocytic thyroid tumors. In our study, 60% of patients harbored mutations in mitochondrial DNA-encoded subunits of Complex I (either missense or nonsense mutations). These mutations were maintained in paired lymph node metastases, suggesting positive selection for Complex I loss in the context of HCTC. This finding stands in contrast to findings of other groups that demonstrated that when human triple-negative breast cancer xenografts were implanted into mice, resulting spontaneous lung metastases exhibited higher tricarboxylic acid (TCA) flux than their paired primary mammary xenografts (Bartman et al., 2023). Cell lines made from HCTC patient-derived xenografts have also been demonstrated to be respiration incompetent (Frank et al., 2023).

HCTC's inability to perform cellular respiration raises the possibility that this disease might harbor targetable metabolic liabilities. Our lab has previously demonstrated that the

lactate dehydrogenase (LDH) reaction is a potential target for HCTC treatment; HCTC, due to its Complex I-null status, is unable to regenerate NAD+ from NADH through the electron transport chain and is therefore overly reliant upon the NAD+ regenerated through the conversion of lactate to pyruvate via LDH (Frank et al., 2023). We posited that given the existence of previously documented nutrient auxotrophies, it was possible that other nutrient auxotrophies exist in HCTC due to its inability to perform cellular respiration and endeavored to perform a screen to discover novel auxotrophies resulting from loss of Complex I function. We also wanted to ask whether we could uncover novel genetic vulnerabilities of HCTC through unbiased CRISPR/Cas9 screening.

3.2 Results

3.2.1 Nutrient auxotrophy screening

In order to conduct our nutrient auxotrophy screen in a higher-throughput fashion, I developed an imaging-based assay to count cell nuclei as a proxy for proliferation in the absence of various nutrients. I utilized the genetic editing technique known as CRISPaint to tag the HIST1H4C histone protein with mClover in 237, our HCTC cell line, as well as in TPC, our respiration-competent papillary thyroid cancer cell line (Figures 5A-C) (Schmid-Burgk et al., 2016).

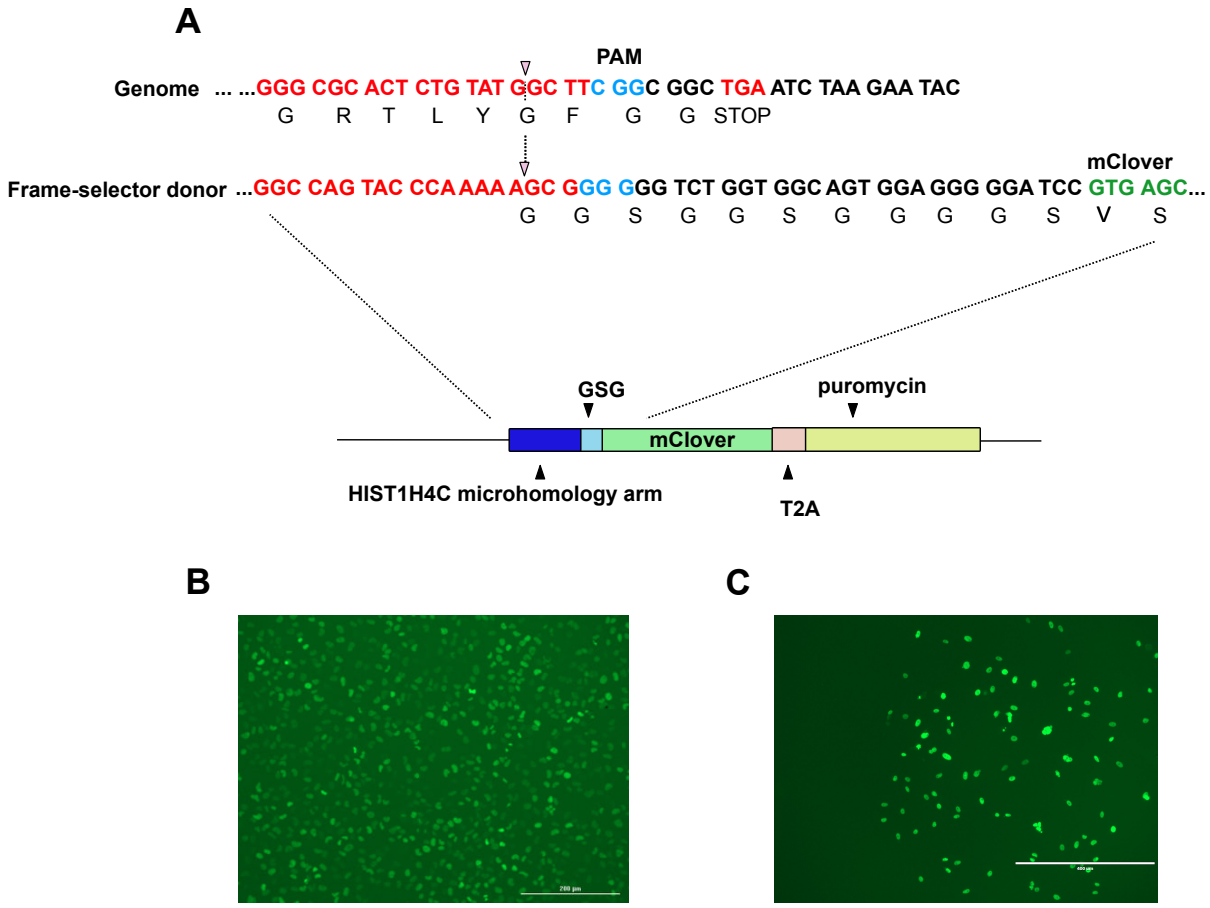

Figure 5. CRISPaint tagging of HIST1H4C. A) Schematic of tagging C-terminal locus of HIST1H4C with mClover protein. B) TPC HIST1H4C mClover cell nuclei are visible using fluorescent microscopy. C) 237 HIST1H4C mClover cell nuclei are visible using fluorescent microscopy.

In order to image the cells, I opted for live cell imaging using the Cytation5 plate reader. I developed a workflow whereby the Cytation5 would systematically image fluorescently tagged nuclei in each well. After automated pre-processing and deconvolution, whereby the background was darkened to improve signal-to-noise ratio of the tagged nuclei, I systematically fed the images through a Cytation5 program that automatically counted the tagged nuclei in each image (Figure 6A). I validated the assay by growing TPC and 237 in pyruvate-free media and demonstrated that the assay detected 237's growth arrest and TPC's

lack of growth defect when grown in the absence of pyruvate (Figure 6B). After validating the assay, I commenced the nutrient auxotrophy screen. I chose to assay the nutrients that were present in HPLM (human plasma-like media) for both physiologic relevance as well as logistic ease.

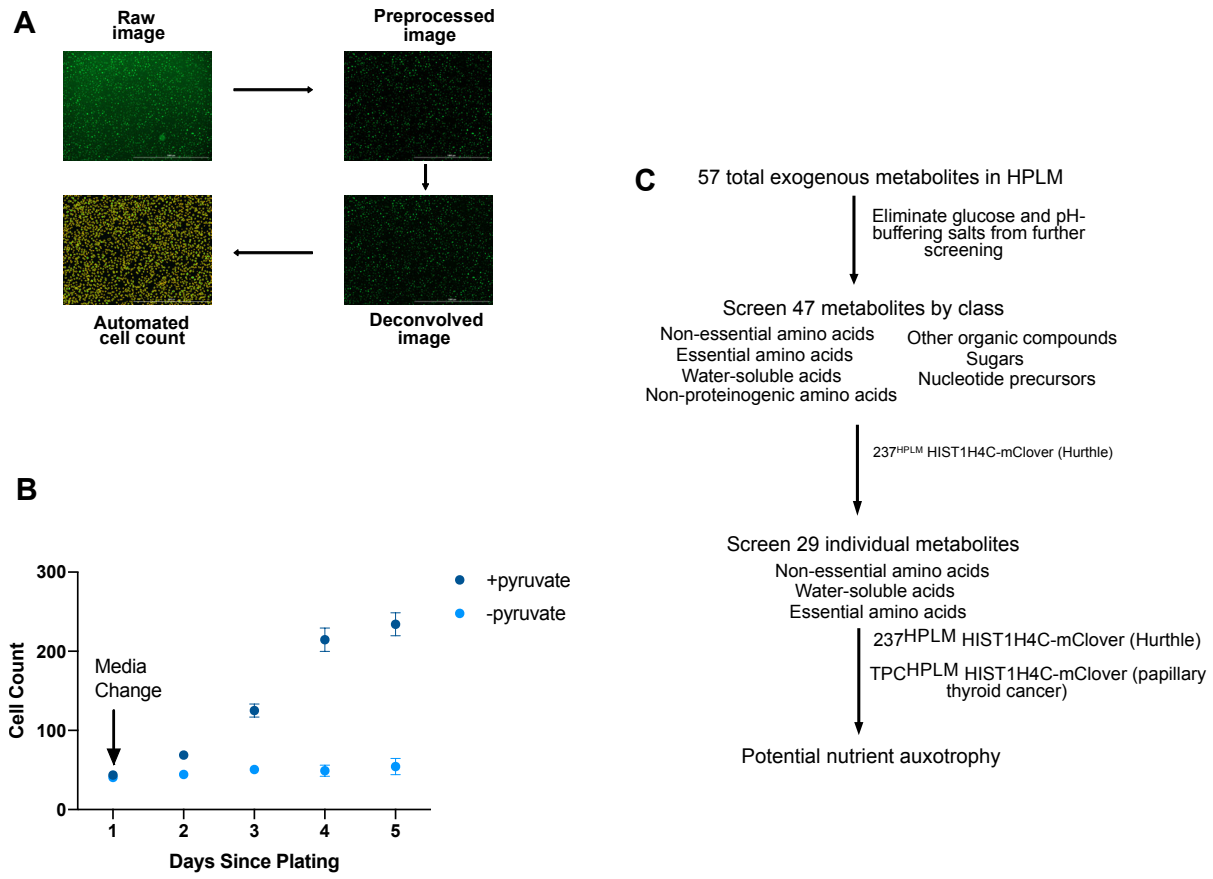

Figure 6. **Validation of nuclei counting assay.** A) Workflow of systematic cell imaging and automated nuclei counting. B) Automated nuclei counting method can detect 237 pyruvate auxotrophy. C) Screening funnel for metabolites.

The exogenous metabolites in HPLM are described in various functional pools, so I first screened each pool by systematically removing each pool from HPLM and determining the presence of absence of a growth defect in 237. I did not proceed screening the metabolites in any pool whose absence did not inhibit 237 proliferation (Figure 6C).

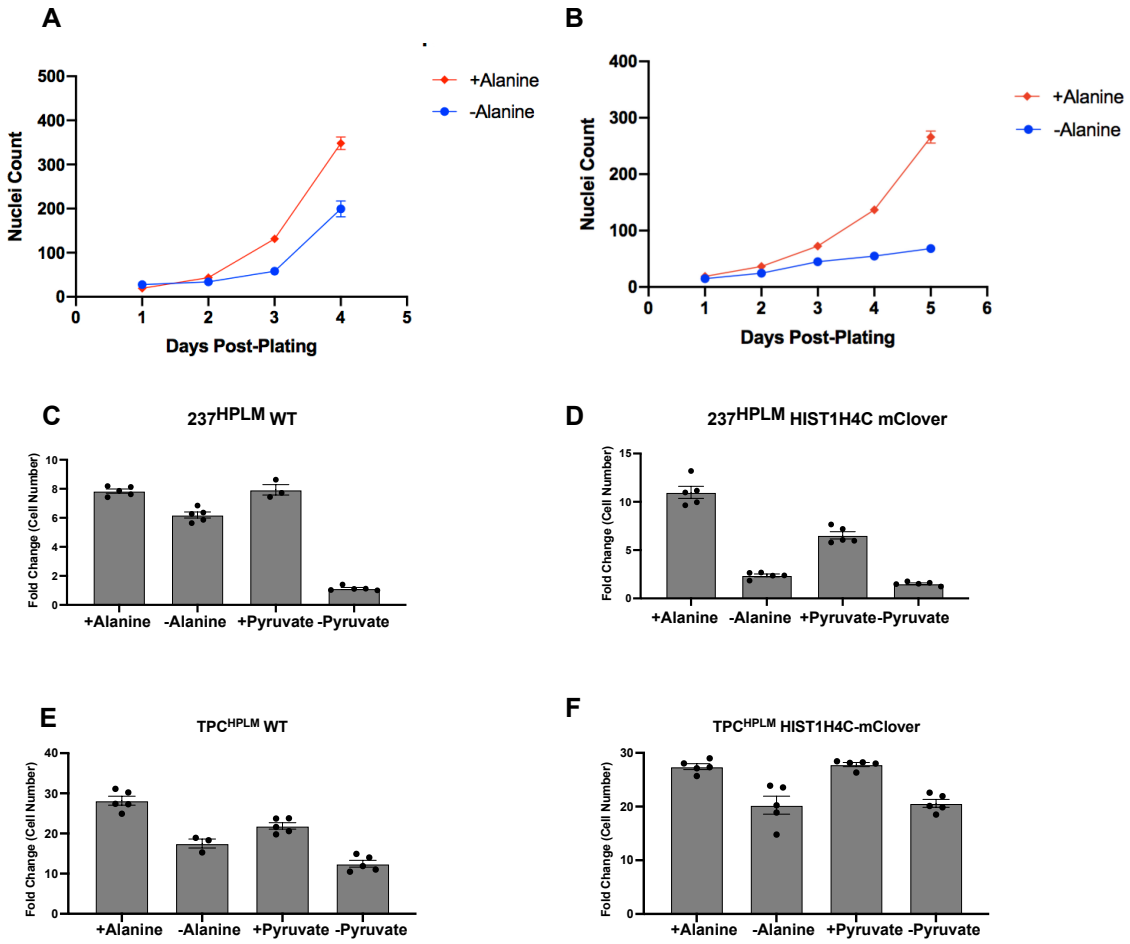

Figure 7. 237 is not auxotrophic for alanine. A) Growth curve of TPC HIST1H4C mClover. B) Growth curve of 237 HIST1H4C mClover. C) Cell count of 237 wildtype in HPLM media. D) Cell count of 237 HIST1H4C mClover in HPLM media. E) Cell count of TPC wildtype in HPLM media. F) Cell count of TPC HIST1H4C mClover in HPLM media.

I then screened the individual exogenous metabolites in each pool whose absence negatively affected 237 growth. I defined a nutrient auxotrophy in 237 as a metabolite whose absence inhibited growth of 237 but did not inhibit growth of TPC. Initially, I found that 237 could not proliferate in the absence of alanine whereas TPC did not exhibit a growth defect in alanine-free media (Figures 7A-B). However, I then wanted to validate the phenotype in our parental 237 cell line and found that wildtype 237 did not exhibit a growth defect in alanine-

free media (Figure 7C-F). I concluded that the alanine auxotrophy was therefore an artifact limited to the screening cell line and not representative of 237 and HCTC biology.

3.2.2 In vitro and in vivo genetic screening of HCTC

As our group is also interested in uncovering genetic vulnerabilities of HCTC, we performed a genome-wide CRISPR/Cas9 screen that revealed glycolysis and lactate dehydrogenase-driven NAD+ regeneration as a targetable vulnerability in HCTC (Frank et al., 2023). To follow up on other hits from this genome-wide screen, I performed a series of targeted CRISPR/Cas9 screens to further narrow down potential genetic vulnerabilities of HCTC. Our goal was to further screen genes that both had an effect on 237 proliferation as well as selectively impaired 237 proliferation relative to our TPC control.

I devised a screening funnel where I selected candidate genes for effect size as well as selectivity (Figure 8A). I selected genes that dropped out at least twofold in the 237 genome-wide CRISPR screen and, from that pool, only selected genes that dropped out at least 1.5-fold more in the 237 condition relative to the TPC condition. Finally, I screened out pan-essential genes by their DepMap score, as our goal was to identify a HCTC-specific genetic vulnerability. These screening filters resulted in a library of 353 genes. I generated a custom CRISPR screening library with all 353 candidate genes and screened this library in our 237, XTC.UC1, and 946 HCTC cell lines as well as TPC and another poorly differentiated thyroid cancer cell line 354 (Figure 8B). Gene performance correlated well between the 3 HCTC cell lines (Figure 8C). As 237 is respiration-deficient, I decided to perform our targeted CRISPR screening in both RPMI and HPLM media to account for any phenotypes that might be context-dependent. To determine whether any genes in our targeted library might be

dependent upon Complex I loss, we also screened this library in our 237 cell line +/- Ndi1, a monomeric NADH dehydrogenase from yeast.

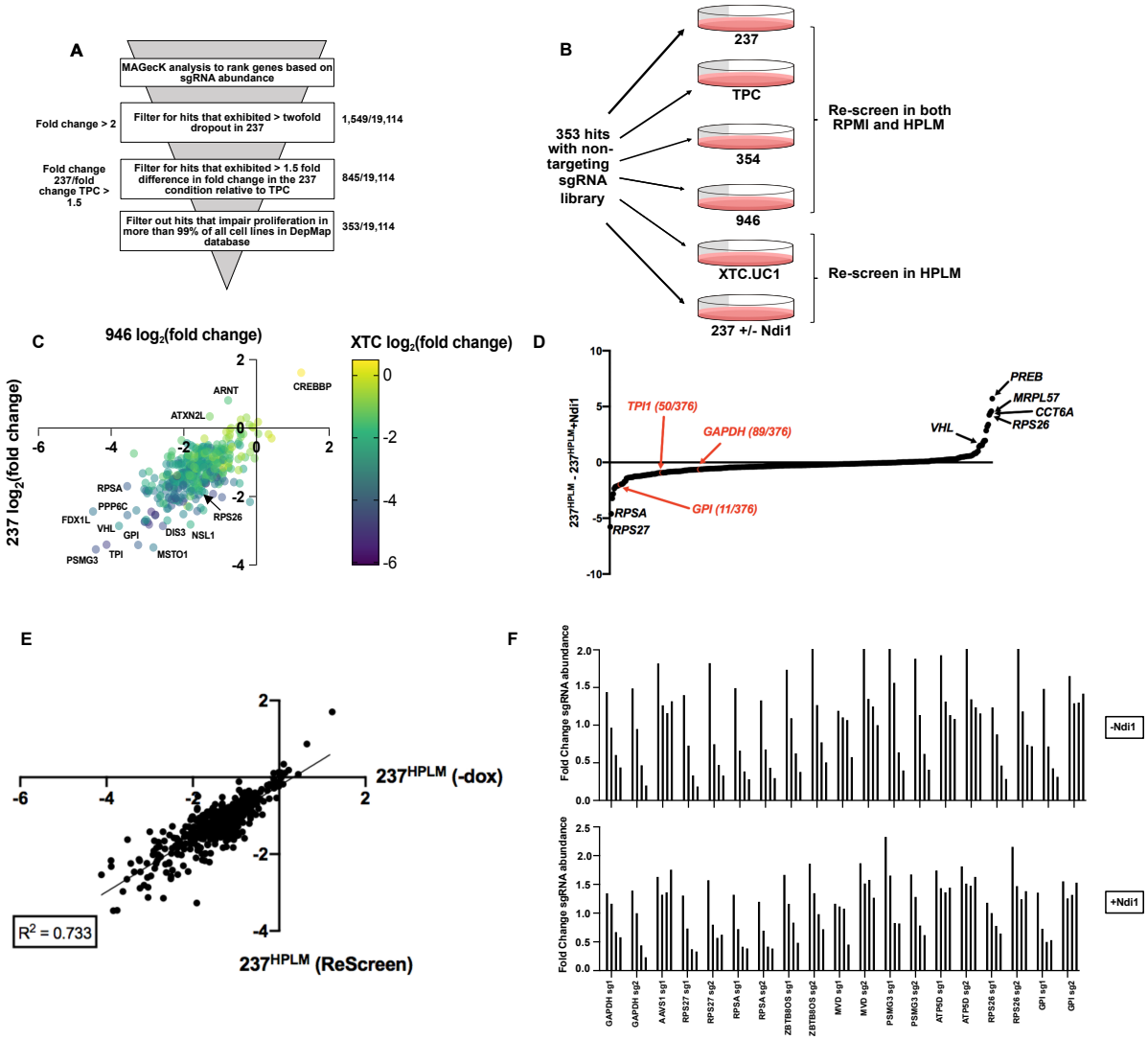

Figure 8. Overview of *in vitro* HCTC CRISPR screening. A) Screening funnel used to select genes for targeted CRISPR screening library. B) Schematic of screening conditions. C) Comparison of gene performance between HCTC cell lines 237, 946, and XTC.UC1. D) Difference in fold-change between genes +/- Ndi1. E) Comparison of gene performance in 237 -Ndi1 screen versus 237 wildtype screen. F) Fold change in sgRNA abundance.

Gene performance in the 237 -Ndi1 condition correlated well with gene performance in the 237 wildtype screen, lending confidence that the screen's results were both

reproducible and biologically relevant (Figure 8E). However, I did not find that restoration of Complex I function via Ndi1 expression significantly changed the performance of the genes in our targeted CRISPR library. To verify our screening results, I performed a CRISPR/Cas9 competition assay where I screened the top hits from the 237 +/- Ndi1 screen. I cloned sgRNA sequences of top hits into lentiCRISPR mCherry and transduced lentivirus made from those lentiCRISPR constructs into 237 cells. Starting from three days post-transduction, I used the Guava benchtop flow cytometer to monitor the percentage of cells expressing mCherry (and, thereby, the percentage of cells that harbored guides of interest). None of the screening hits behaved markedly differently +/- Ndi1 (Figure 8F).

In order to ascertain which genes from our targeted *in vitro* CRISPR screening might be important for 237 xenograft growth, I performed an *in vivo* CRISPR screen. To determine the size of the in vivo library I could feasibly screen in 237 xenografts, I relied upon an experiment performed by a previous graduate student in the lab, Anderson Frank. He injected either 1 or 2 million 237 cells infected with a 363,113 guide barcode library as subcutaneous xenografts in NSG mice. Upon sequencing the resulting tumors, we were able to recover roughly 5000 barcodes from tumors seeded with 2 million cells (Figure 9B). Assuming a desired coverage of 1000X, we estimated that we could screen 5 sgRNAs per xenograft. For the sake of logistics, we chose to conduct the screen in 25 mice and thus over 50 xenografts. 50 xenografts would allow us to screen 250 sgRNAs. At four sgRNAs per gene, we calculated that 50 xenografts would allow us to screen approximately 60 genes.

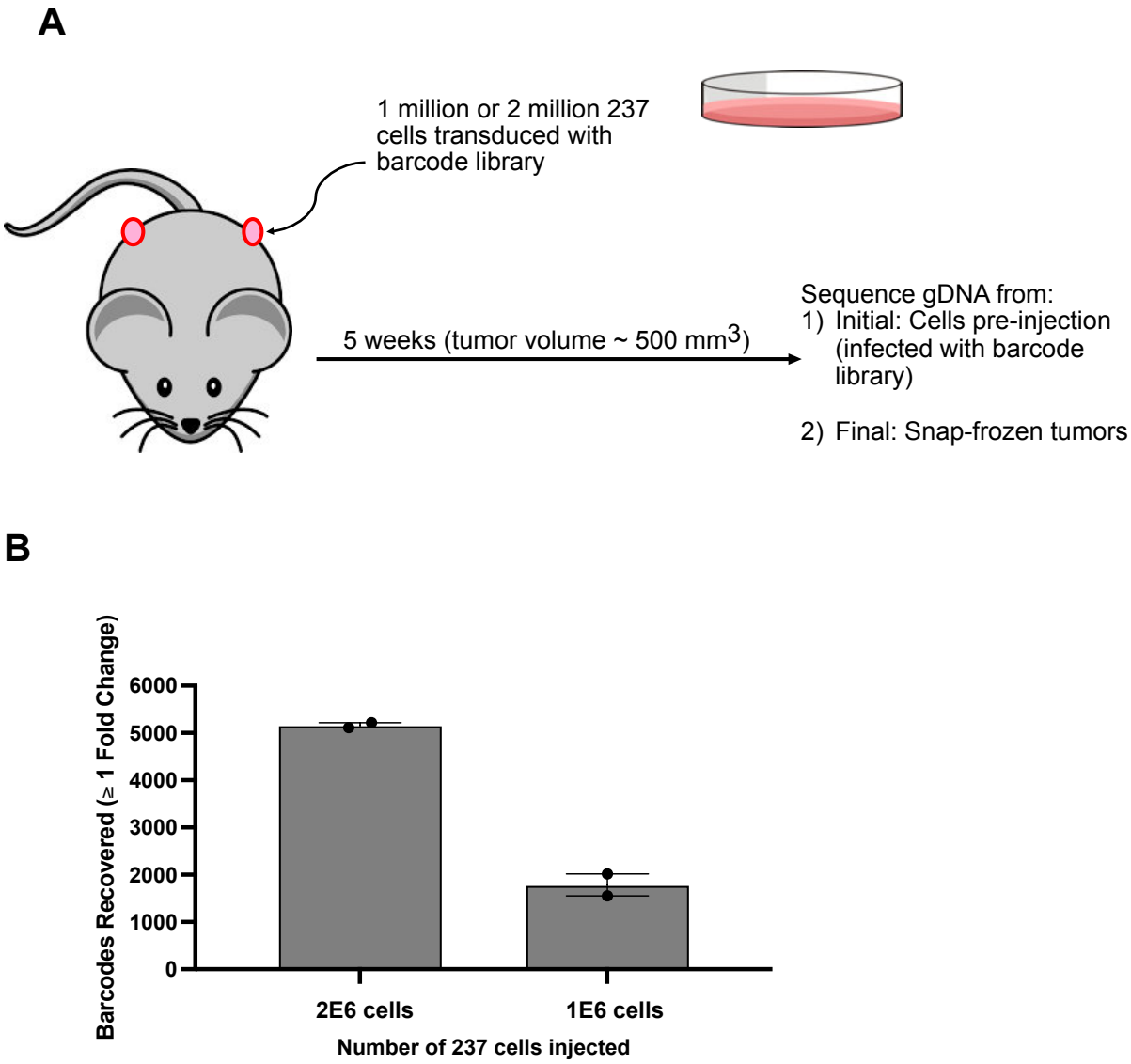

Figure 9. Determination of sgRNA coverage for in vivo CRISPR screening. A) Workflow for determining sgRNA coverage in 237 xenografts. B) Number of barcodes recovered per xenograft whose abundance did not decrease in the final xenograft relative to the initial barcode library.

I ranked our hits by fold dropout in the 237 HPLM condition and selected the top 50 performers that also dropped out more than threefold in the 237 RPMI screen. I reasoned that the genes that would have the greatest likelihood of being important for 237 xenograft

growth would have dropped out significantly in my 237 screening regardless of media condition. 10 of the genes that dropped out in the 237 RPMI screen but were not among the highest-performing genes in the 237 HPLM targeted screening. The remaining 2 genes dropped out in the 237 HPLM screen but not the 237 RPMI screen. I also included 15 non-targeting sgRNAs to ascertain whether stochastic dropout occurred in the process of the xenograft experiment (Figure 10A). Each xenograft was comprised of 2 million 237 cells suspended in a 1:1 ratio with Matrigel. 50 xenografts were injected into 25 NOD/SCID (NSG) mice and the experiment was terminated once the xenografts reached an average tumor volume of 300 mm^3.

Xenografts were snap frozen and genomic DNA was extracted from pulverized xenograft tissue using a phenol-chloroform-based extraction method. After receiving the results, I first noted that our non-targeting guide RNAs did not change in distribution from the beginning to the end of the screen (Figure 10B), indicating that we had screened our genes at sufficient coverage to avoid stochastic dropout of guide RNAs that should have had no effect on xenograft proliferation. The glycolytic enzymes *GPI*, *GAPDH*, *TPI1* also dropped out in the *in vivo* screen, further corroborating the lab's previous work showing that glycolysis was a targetable dependency of HCTC (Frank et al., 2023) (Figure 10C).

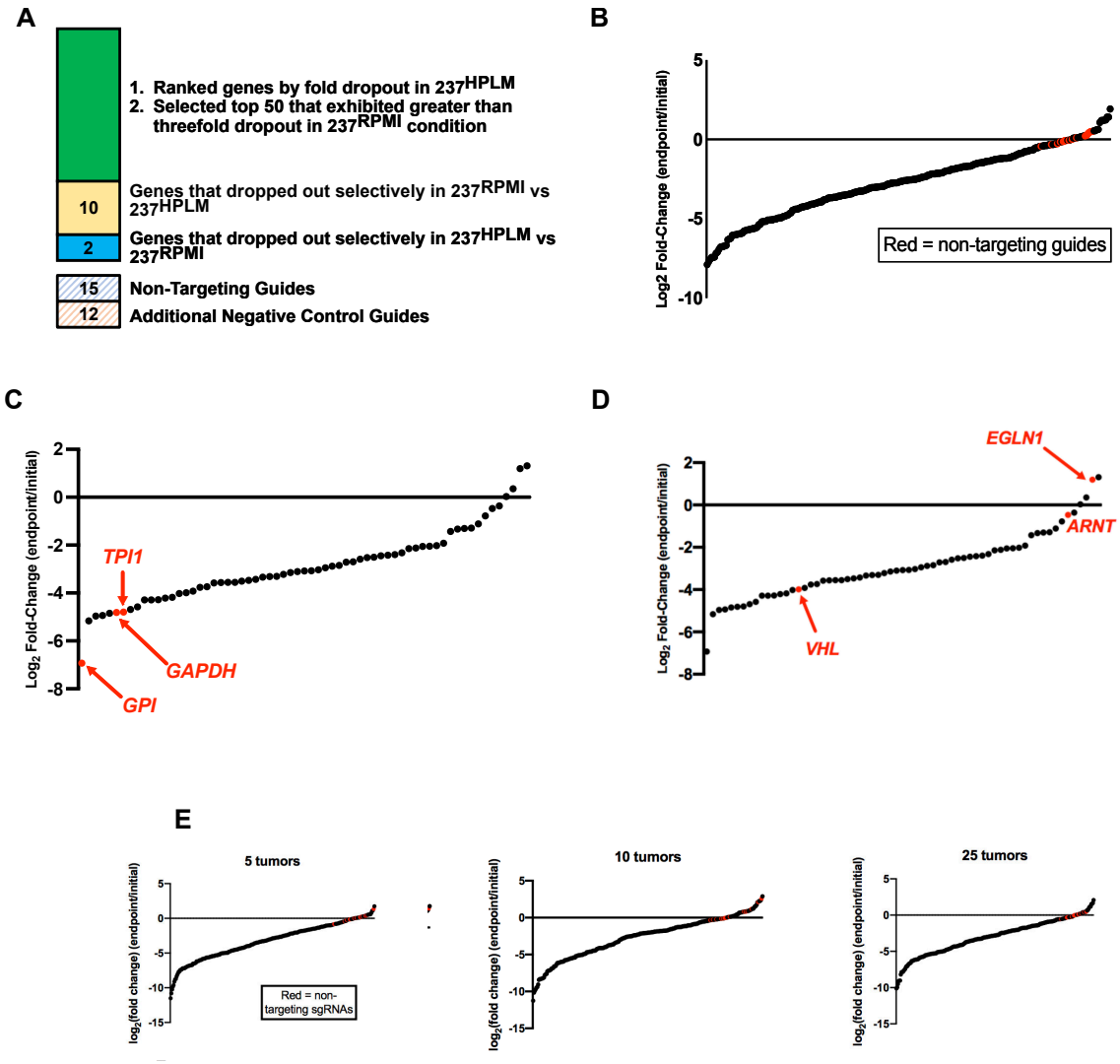

Figure 10. ***In Vivo*** **CRISPR screening results**. A) Inclusion criteria for in vivo CRISPR screen. B) Plot of the $\log_2$(fold change) for individual sgRNAs C) Performance of glycolytic enzymes (red) D) Performance of HIF1α signaling regulators (red) E) Performance of non-targeting sgRNAs throughout tumor dilution experiment.

I was also curious to know how many genes I could feasibly cover in future in vivo screens. To assess the technical limits of future *in vivo* screens done in our 237 model, I extracted genomic DNA individually from all 50 remaining tumors. I submitted pooled samples representing 5, 10, or 25 xenografts for next-generation sequencing and compared

sequencing results to the original *in vivo* CRISPR screen that sampled all 50 xenografts. I found that non-targeting guides performance remained unchanged for the 25 tumor and 10 tumor conditions (Figure 10E). Gene performance was similar between all conditions. These data indicate that in the future each 237 xenograft could feasibly screen 50 sgRNAs per xenograft as opposed to the 5 sgRNAs per xenograft we had initially estimated. These results will be valuable for future in vivo CRISPR screening endeavors using 237 xenografts.

Most interestingly, I noted differential performance of the two known negative regulators of HIF1α signaling, *VHL* and *EGLN1* (Figure 10D). In normoxic conditions, the transcription factor HIF1α is hydroxylated by EGLN1. This hydroxylation creates a motif recognized which allows it to be recognized by the E3 ligase VHL and subsequently targeted for degradation through the proteasome. Guides against *VHL* dropped out in our 237 *in vivo* screen whereas guides against *EGLN1* were slightly enriched. If their effects on 237 xenograft growth were solely through the HIF1α signaling pathway, one would have expected both genes to behave similarly. Our screening results indicated that either *VHL* or *EGLN1* might affect 237 xenograft growth through actions on a non-canonical substrate. Future work will need to be done to validate these screening results and interpret how one or both of these HIF1α signaling regulators impact 237 proliferation.

3.3 Discussion

In the previous section, I outlined a comprehensive screening program to identify potential liabilities in HCTC, both metabolic and genetic. Although the nutrient auxotrophy screen failed to identify any novel nutrient auxotrophies of HCTC, the higher-throughput nuclei counting assay may remain a valuable tool future endeavors into screening

dependencies of HCTC and may even be applied to other cell lines in the future, as the counting assay merely requires knocking in a fluorescent protein at the C-terminus of a gene encoding for a histone. In addition, there exists the possibility that we missed a nutrient auxotrophy if that nutrient was not part of the HPLM media formulation.

After conducting a series of CRISPR/Cas9 screens to identify genetic vulnerabilities of our HCTC cell line 237, our CRISPR screening efforts have revealed a number of gene candidates that are necessary for 237 proliferation both *in vitro* and *in vivo*. We were heartened to see that sgRNAs targeting the glycolytic enzymes *GPI*, *TPI1*, and *GAPDH* all dropped out in the *in vivo* CRISPR screen as it aligned with our prior work demonstrating that inhibiting lactic acid fermentation, one of the endpoints of glycolysis, prevents 237 xenograft growth (Frank et al., 2023).

I also hope that future work will be done to follow up on the hits that resulted from the 237 *in vivo* screen. While it was disappointing that none of the hits from the targeted screens appeared to be Complex I-dependent (as evidenced by the CRISPR competition assays), it remains possible that at least one of the genes that dropped out in the *in vivo* screen might still be a HCTC-specific liability particularly given that the majority of genes performed similar in the three targeted CRISPR screens across our three HCTC cell lines 237, 946, and XTC.UC1 (Figure 4C).

In particular, further investigation will be necessary to elucidate the roles of either *EGLN1* or *VHL* on 237 xenograft growth and whether either one of those genes is acting in a manner independent of HIF1α signaling. One outstanding question remains why EGLN and VHL performed so different in the *in vitro* screening as opposed to the *in vivo* screening. In

all *in vitro* screening I performed, guides against both *EGLN1* and *VHL* drop out, indicating that constitutive HIF1α signaling has a negative impact on 237 growth in culture. This stands in contrast to my results from the in vivo screening where guides against VHL mimicked their in vitro performance but guides against EGLN1 appeared to have a completely different effect on 237 proliferation *in vivo*. As the sgRNA sequences we used were the same between both phases of CRISPR screening, I suspect that an element present in the 237 xenograft environment that is absent in the tissue culture environment led to our disparate results. As screening in HPLM did not change the performance of most of our genes, including *VHL* and *EGLN1*, I don't believe that metabolite availability was a major factor in our conflicting results.

I have conducted preliminary experiments to follow up on our EGLN and VHL results, however I have run into difficulties reproducing our screening results. While I am able to reproduce our CRISPR screening results *in vitro*, I was unable to reproduce our in vivo results. When I injected *VHL* KO, *EGLN1* KO, and *HIF1α* KO 237 xenografts back into NOD-SCID mice, both *VHL* KO and *EGLN1* KO caused 237 xenografts to grow faster than *AAVS1* controls. Both technical and biological challenges may have impeded my validation efforts – there were low levels of residual protein in my knockout cell lines prior to injection (data not shown). Thus, these cell lines would be more accurately referred to as "knockdown" cell lines as opposed to "knockout" cell lines. Prior to any repeat experiments, I would attempt to plate single-cell clones to achieve clean knockouts of the genes in question. Another hypothesis is that my cell lines adapted quickly to the knockout, causing the xenograft experiment to yield different results than the screening. In the CRISPR screen,

I cultured the cells with the sgRNA library for seven days and then injected the cells as xenografts. My initial xenograft validation experiments were done with knockdown cell lines that had been in culture for over 21 days prior to injection. One future method to avoid allowing cells to adapt would be to introduce a doxycycline-inducible Cas9 system into my 237 cells prior to injecting the cells as xenografts. I would then feed the mice doxycycline chow to induce Cas9 so that the cells could avoid adapting to sgRNA expression and Cas9 cutting while in culture. I hope that my efforts will serve as a resource for my lab's future endeavors to investigate the biology of HCTC.

CHAPTER FOUR

Characterization of Novel Genetically Engineered Murine Models of Complex I-Deficient Thyroid Cancer

4.1 Introduction

HCTC is not the only thyroid cancer subtype that harbors widespread loss of Complex I. A group in Italy recently found that a cohort of tall cell variant – papillary thyroid cancer (TCV-PTC) patients all harbored loss of function mutations in mitochondrial DNA-encoded subunits of Complex I. They verified that tumors from TCV-PTC patients did not express Complex I. Furthermore, they used electron microscopy to show that TCV-PTC tumor cells harbored the same accumulation of malformed mitochondria that is also found in HCTC patients (Tsybrovskyy et al., 2022).

Papillary thyroid cancer (PTC) is by far the most common subtype of thyroid cancer, accounting for 84% of all thyroid cancers (Lim et al., 2017). Most PTC patients do well clinically after the standard treatment of surgical resection and adjuvant radioiodine; a recent study of PTC patients showed that there was a 97% rate of overall survival (Ito et al., 2018). TCV-PTC comprises between 1-3% of all PTC cases (Ghossein & Livolsi, 2008; Longheu et al., 2020). TCV-PTC is an aggressive form of PTC; compared to classical PTC (cPTC), TCV-PTC exhibits lower rates of radioiodine (RAI) uptake, higher metastasis rates, and poorer five-year survival outcomes (Longheu et al., 2020).

PTC is driven by activating mutations in the mitogen-activated protein kinase (MAPK) signaling cascade (Kondo et al., 2006). This signaling cascade is comprised of a

series of serine/threonine kinases that transduce signals from external stimuli after interacting with a membrane-bound protein in the Ras/Rho GTPase family. The MAPK kinases are each grouped into a module of three proteins that work in concert: a MAP kinase kinase kinase (MAPKKK), a MAP kinase kinase (MAPKK), and a MAP kinase (MAPK). The ERK1/2 module is one of the most well-studied MAPK groups. The module's signaling pathway begins with the A-raf, B-raf, and Raf-1 MAPKKKs. These MAPKKK's phosphorylate and activate the MAPKK's MEK1 and 2. MEK1/2 activates the MAPK's ERK1/2 by phosphorylating both the threonine and tyrosine within the Thr-X-Tyr motif within the activation loop of ERK1/2 (Cargnello & Roux, 2011). MAP kinase mutations that drive constitutive activation are common oncogenic drivers in not only papillary thyroid cancer but also other cancers like melanoma and ovarian cancer (Tran et al., 2011; Zhang et al., 2016). TCV-PTC is universally driven by the BRAF V600E activating mutation within the MAPK pathway (Cantwell-Dorris et al., 2011; Tsybrovskyy et al., 2022).

Our lab has previously generated two autochthonous mouse models of thyroid cancer: a *TPOCreER*; $Braf^{CA/+}$ (TB) and a *TPOCreER*; $Braf^{CA/+}$; $p53^{FL/FL}$ (TBP) mouse (McFadden et al., 2014). Thyroid peroxidase (TPO) is the rate-limiting enzyme responsible for generating the thyroid hormones T3 and T4. TPO oxidizes iodide (I_2) to the iodine radical (I^-); iodine is extremely reactive and easily modifies tyrosine residues on their phenol R-groups (Ruf & Carayon, 2006). Iodine radicals in thyroid follicular cells modify the tyrosine residues on the thyroglobulin protein within thyroid follicular cells, a process known as "iodide organification." TPO expression is solely restricted to thyroid follicular cells. Therefore, by placing the *CreER* allele under the thyroid peroxidase (TPO) promoter, Cre

expression can also be restricted solely to the thyroid. Cre expression is induced by two intraperitoneal injections of 20mg/ml tamoxifen 24 hours apart. Upon Cre induction, cells with the Braf CA (Cre-Activated) allele will express mutant Braf V600E. TB mice develop papillary thyroid cancer starting at around 6 months post-treatment. TBP mice first develops papillary thyroid cancer that then undergoes a process seen in human patients called "anaplastic transformation," where the tumor de-differentiates into anaplastic thyroid cancer (Hunt et al., 2003; Khairy, 2009; Kondo et al., 2006).

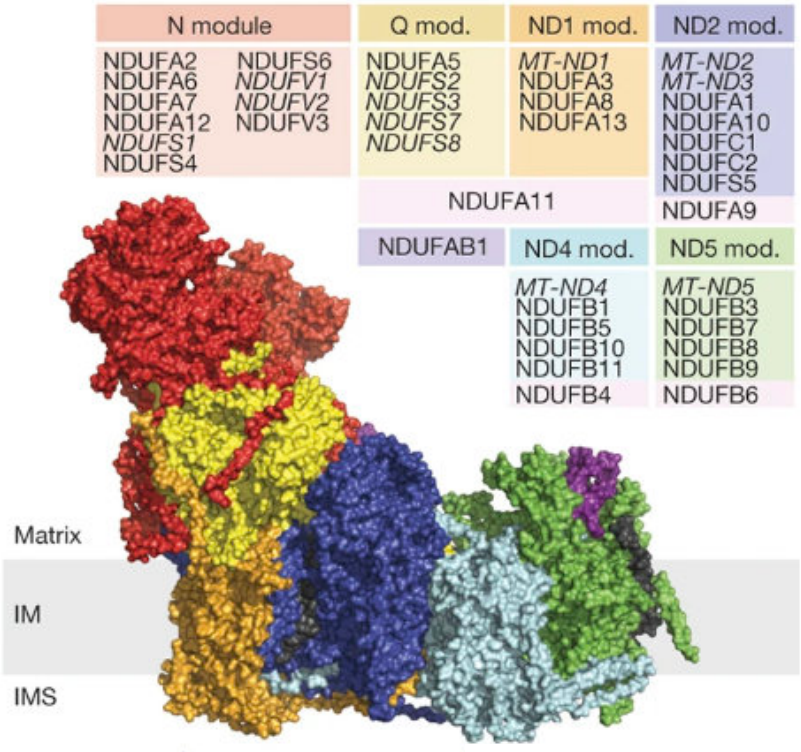

Figure 11. Structure of *Homo sapiens* Complex I. Adapted from Stroud et al 2016.

Previous attempts in the lab to generate a murine model of HCTC using disease-relevant mutations had not been successful. Our lab had also generated an allele to induce Complex I loss in a Cre-dependent manner (Wang et al., 2022) (Figure 12). Complex I is a

multi-subunit NADH dehydrogenase. and the efficiency of Cre-dependent recombination decreases with increasing genetic distance between loxP sites (Zheng et al., 2000). We decided to target a Complex I subunit encoded by the nuclear genome as mtDNA remains more technically challenging to manipulate. Newer mtDNA editing technologies like mitochondrial base editing were not published until 2020 (Mok et al., 2020). Upon literature review, we found a previous study which demonstrated that TALEN-mediated deletion of Ndufa9's N-terminal mitochondrial targeting sequence results in loss of Complex I function due to Ndufa9's role in stabilizing the matrix arm of Complex I. (Stroud et al., 2013; Stroud et al., 2016). Our Ndufa9 allele demonstrates complete protein ablation upon Cre induction and Ndufa9 loss is sufficient to result in a failure to perform cellular respiration (Wang et al., 2022).

In earlier experiments, we found that thyroid-specific Complex I loss and p53 loss (*TPOCreER*; $Ndufa9^{FL/FL}$; $p53^{FL/FL}$) were not sufficient to induce HCTC (data not shown). Upon seeing the findings of Tsybrovskyy et al, we realized if we combined our Cre-dependent Ndufa9 allele with our pre-existing Cre-inducible thyroid cancer mouse models, we would create an autochthonous model of Complex I loss in the setting of Braf-driven thyroid tumorigenesis using patient-relevant mutations. Using this mouse model, I began to investigate how Complex I loss could affect thyroid cancer progression.

4.2 Results

4.2.1. Murine anaplastic thyroid cancer does not tolerate Complex I loss

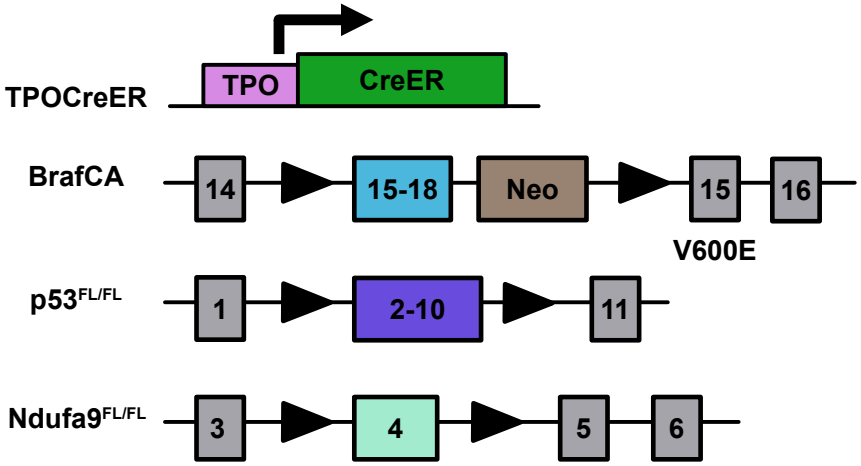

Figure 12. Schematic of alleles.

Our lab had previously developed two mouse models of Braf-driven thyroid tumorigenesis: *TPOCreER*; *Braf*$^{CA/+}$ (TB) and *TPOCreER*; *Braf*$^{CA/+}$; *p53*$^{FL/FL}$ (TBP). We introduced our *Ndufa9*$^{FL/FL}$ allele to both models, generating *TPOCreER*; *Braf*$^{CA/+;}$ *Ndufa9*$^{FL/FL}$ (TBN) and *TPOCreER*; *Braf*$^{CA/+}$; *p53*$^{FL/FL}$; *Ndufa9*$^{FL/FL}$ (TBPN) mice.

Genotype abbreviation	Full Genotype
TB	*TPOCreER*; *Braf*$^{CA/+}$
TBN	*TPOCreER*; *Braf*$^{CA/+;}$ *Ndufa9*$^{FL/FL}$
TBP	*TPOCreER*; *Braf*$^{CA/+}$; *p53*$^{FL/FL}$; *Ndufa9*^{WT}
TBPN	*TPOCreER*; *Braf*$^{CA/+}$; *p53*$^{FL/FL}$; *Ndufa9*$^{FL/FL}$

Table 2. Table of genotype abbreviations.

I compared rate of murine anaplastic thyroid cancer (mATC) development in TBP and TBPN mice by inducing tumors with intraperitoneal tamoxifen when the mice were 8-12 weeks of age. I followed the treated mice over time and monitored the mice weekly for physical symptoms of tumor burden including but not limited to shortness of breath, low body score condition, decreased physical activity, and wheezing (a proxy for whether the induced tumor had begun to invade into the trachea). I euthanized the mice when their overall condition indicated severe tumor burden and used that date as the endpoint for survival. Surprisingly, TBPN mice exhibited similar survival rates to TBP mice. Both TBPN and TBP mice developed ATCs at around 6 months post-treatment (Figure 13). I was initially surprised by this finding as I had not expected a tumor model to be completely insensitive to Complex I loss.

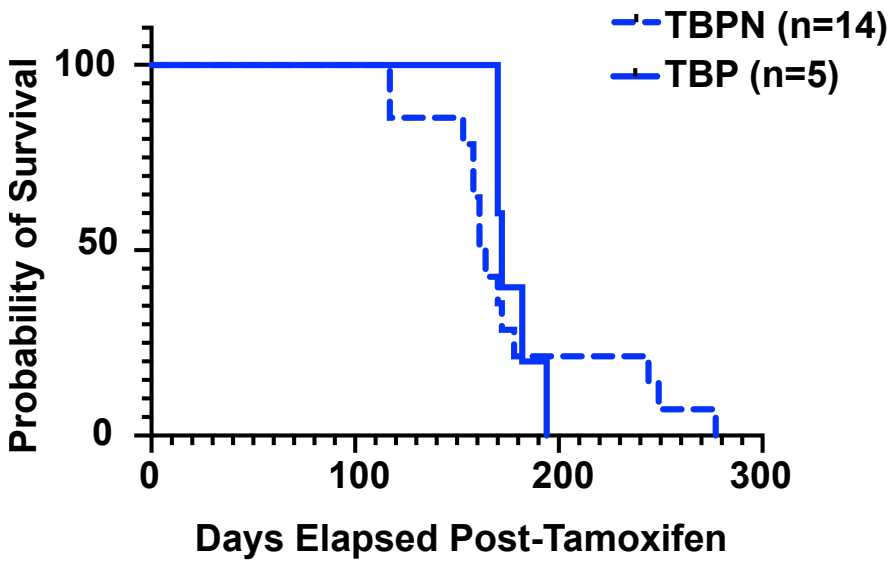

Figure 13. Kaplan-Meier survival curve of TBP and TBPN mice. Comparison between TBP and TBPN.

The ATCs resulting from TBPN mice and TBP both morphologically established ATCs (upon H&E, tumors were characterized by spindly, mesenchymal cells) (Figure 14A). However, the ATCs from TBPN mice did not lose Complex I by immunohistochemistry (IHC) staining against the Ndufs4 subunit of Complex I (Figure 14A). My initial surprise was based upon the assumption that the TBPN ATCs were Complex I-null. These findings suggested that, in the setting of anaplastic thyroid cancer, there is a selective pressure against Complex I loss.

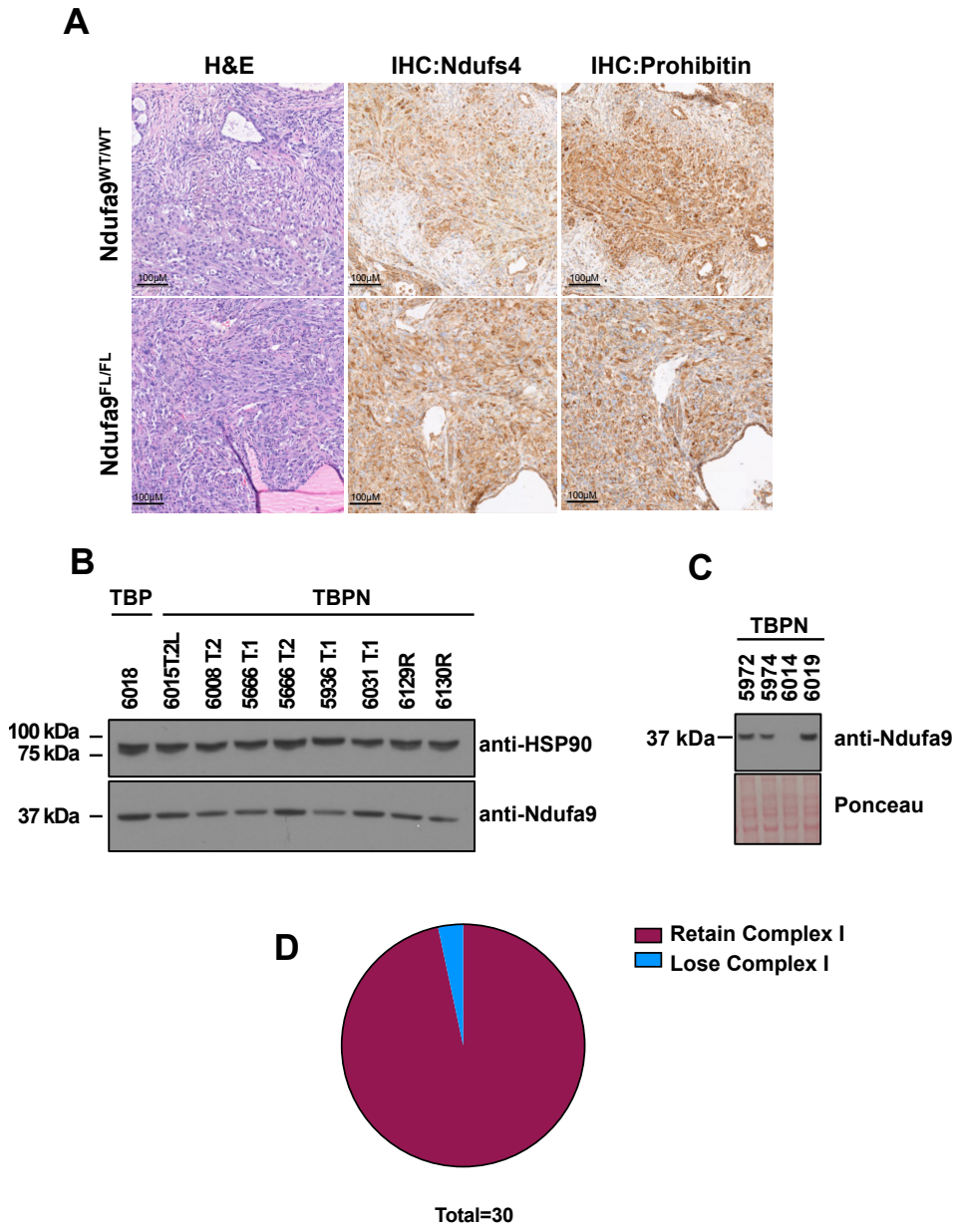

Figure 14. ATCs from TBPN mice retain Complex I. A) Representative histology from TBP (top panel) and TBPN (bottom panel) ATCs. B) Representative Western blot of 8 TBPN ATC cell lines. C) Western blot of 4 TBPN ATC cell lines. D) Diagram of cell lines Complex I status as assessed by Western blot.

I further verified that TBPN ATCs retained Complex I by assessing Complex I status of cell lines generated from TBPN ATCs both by genotyping as well as Western blotting (Figure 14B-D). Of the 30 cell lines generated from TBPN ATCs, 29 cell lines either did not

recombine or only partially recombined the Ndufa9 allele. Only 1 cell line fully recombined Ndufa9 and lost Ndufa9 expression by Western blot (Figure 14D).

When I harvested PTCs from both TBP and TBPN mice, however, I observed Complex I-null TBPN PTCs (Figure 15). This stands in contrast with TBPN ATCs. Together, these results suggest that while PTCs can proliferate even after they have lost Complex I, ATCs either cannot arise from Complex I-null precursor cells or fail to proliferate in the setting of Complex I loss. This data raises the possibility that a unique feature of PTC biology permits tumor proliferation in the setting of Complex I loss.

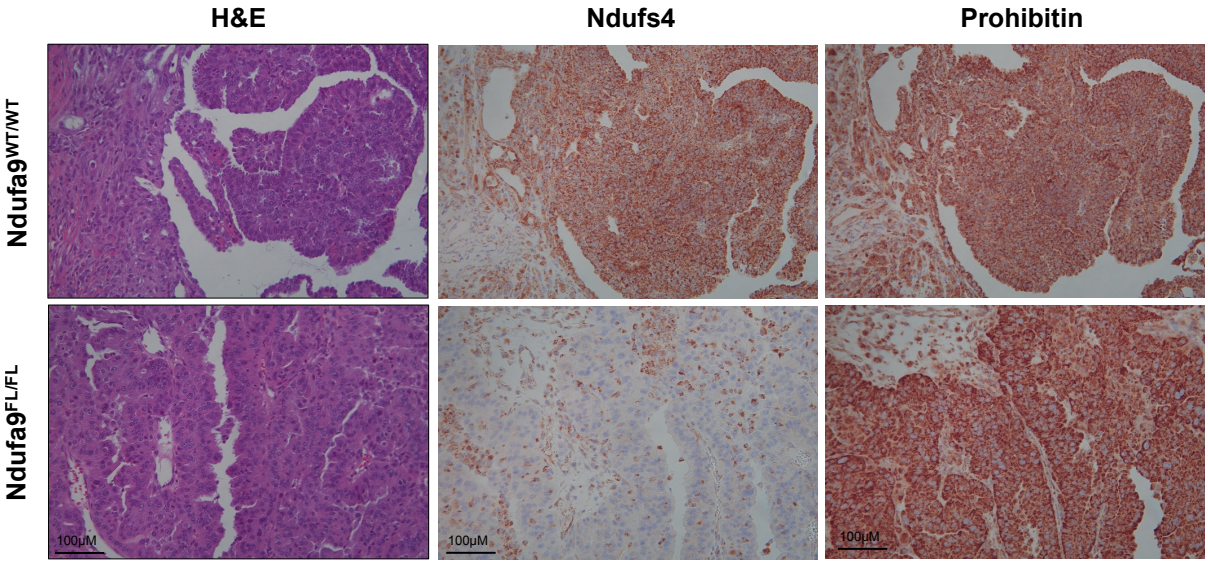

Figure 15. PTCs from TBPN mice lose Complex I. Representative histology.

4.2.2 Complex I loss is not tolerated in rhabdomyosarcoma and lung adenocarcinoma

After our initial results in the setting of thyroid tumorigenesis, I next wanted to ask whether TBP and TBPN mice provide a clear isogenic system to study Complex I dependence of various tumor types. I administered adenoviral Cre to TBP and TBPN mice

either intratracheally to induce lung adenocarcinoma or intramuscularly in the thigh to induce rhabdomyosarcoma (Figure 15A). TBPN mice developed rhabdomyosarcoma at similar rates to TBP mice; both TBP and TBPN rhabdomyosarcomas reached endpoint at approximately 85 days post-Cre infection (Figure 16B) but the TBPN rhabdomyosarcomas were positive for Complex I by IHC staining against Ndufs4 (Figure 16C). Lung adenocarcinomas in TBPN and TBP mice both reached endpoint at approximately 225 days post-Cre infection (Figure 16D). The majority of TBPN lung adenocarcinomas were positive for Ndufs4 by IHC staining as well (Figure 16E).

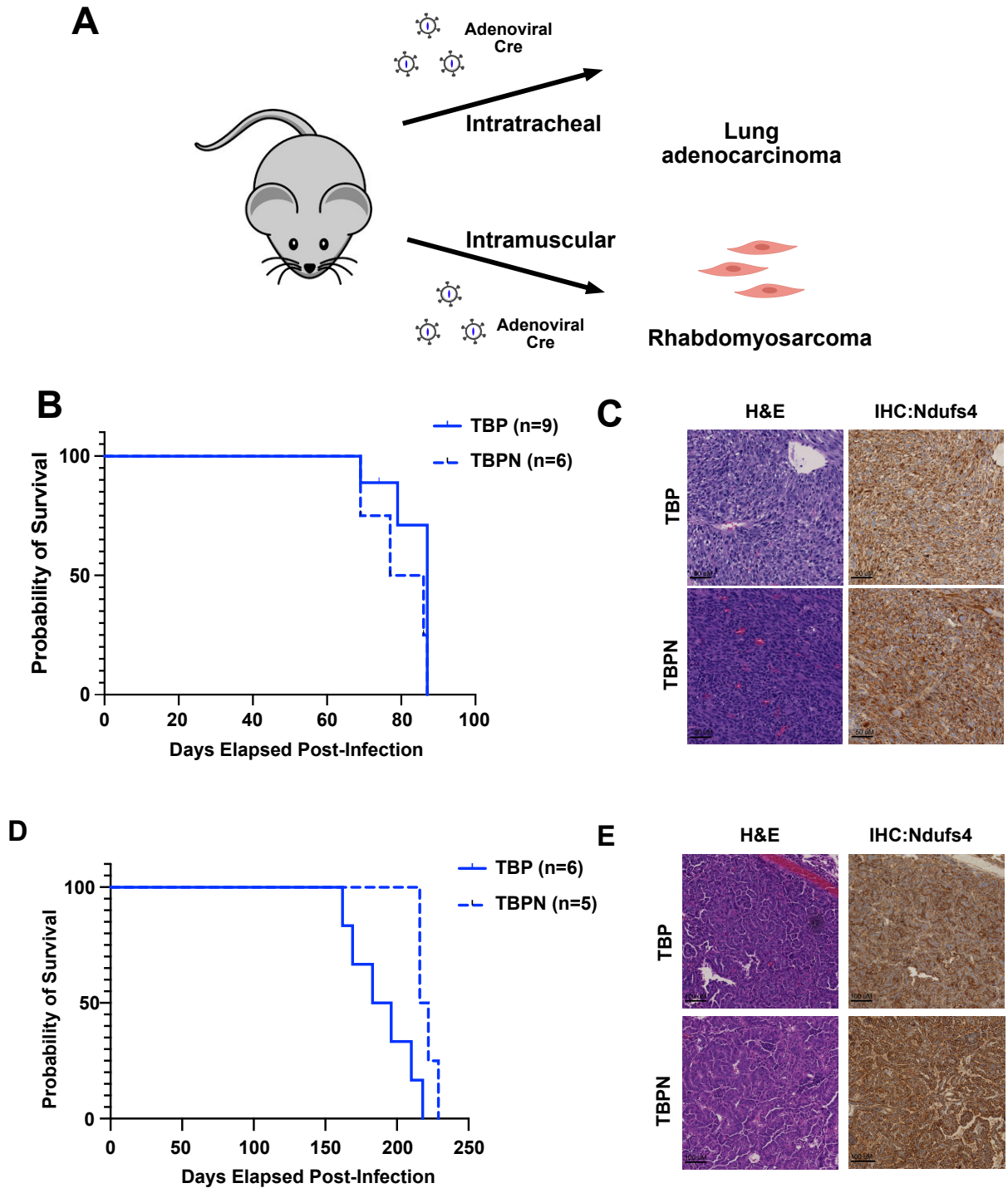

Figure 16. Complex I loss is not tolerated in non-thyroid tumor lineages. A) Schematic of tissue specificity experiment. B) Kaplan-Meier survival curve of TBP and TBPN rhabdomyosarcoma development. C) Representative histology of rhabdomyosarcomas from TBP (n=9) and TBPN (n=6) mice. D) Kaplan-Meier survival curve of TBP and TBPN lung

adenocarcinoma development. E) Representative histology of lung adenocarcinomas from TBP (n=6) and TBPN mice (n=5).

4.3 Discussion

Together, my results suggest that Complex I loss is detrimental to tumorigenesis of anaplastic thyroid cancer as well as non-thyroid cancer lineages lung adenocarcinoma and rhabdomyosarcoma. While the unfavourability of Complex I loss in tumorigenesis has been extensively documented in previous literature (Martinez-Reyes et al., 2020; Sellers et al., 2015; Xie et al., 2016), our TBPN mouse model represents an animal model that could be utilized to study contexts in which Complex I loss is permitted or, in certain contexts, might even promote tumorigenesis. My initial work raises far more questions than answers. Why is the PTC environment so permissive to Complex I loss? What features, if any, of thyroid biology generate an environment that is much more permissive of Complex I loss than other tissues? How are Complex I-null tumors overcoming the metabolic dysfunction that ensues in the setting of ETC dysfunction? If Complex I can offer a proliferative advantage in cases such as TCV-PTC, what are the underlying mechanisms? Could we exploit these mechanisms to develop targeted therapies for Complex I-null tumors?

As anaplastic thyroid cancer is much more aggressive than papillary thyroid cancer, the TBPN model is not the ideal system in which to interrogate the role of Complex I in the setting of papillary thyroid cancer. Based on our model, we observe that anaplastic thyroid cancer comprises the majority of the thyroid tumor at roughly 6 months post-tamoxifen induction. Therefore, our TBPN model only gives us roughly 6 months to observe the effect of Complex I on PTCs before the tumor is taken over by the resulting ATC and the mouse dies as a result of the ATC.

We have also introduced the Ndufa9 allele into *TPOCreER; Braf$^{CA/+;}$ p53^{WT}* (TB) mice, generating *TPOCreER; Braf$^{CA/+;}$ p53^{WT}; Ndufa9$^{FL/FL}$* (TBN) mice. As our mouse model does not progress to ATC in the p53 wildtype background, the TBN mice will be a better system in which to assess the effect of Complex I loss on thyroid tumor progression. I have already induced thyroid tumors in our TB and TBN mice using intraperitoneal tamoxifen. Further work will include harvesting resulting tumors from TBN mice and assessing Complex I status. Using our TBN model, we will be able to assess how Complex I loss impacts tumorigenesis using a variety of metrics such as tumor size, tumor grade, and rate of metastasis. Another group has already demonstrated that Complex I-null xenografts formed from SV40-immortalized thyroid epithelial cells demonstrated a growth advantage over respiration-competent controls (Kotrys et al., 2024). Our TBN model offers a more disease-relevant model to study whether Complex I loss could be advantageous in tumorigenesis.

After probing the effect of Complex I loss on tumor formation and progression, we plan to delve further into the mechanism of how Complex I loss can promote tumorigenesis. Much of the previous work done in the field has focused on finding therapeutic vulnerabilities of Complex I-null cancers; in particular, thyroid cancer like HCTC. Our own group recently published work demonstrating that inhibiting lactate fermentation halted 237 HCTC xenograft growth (Frank et al., 2023). Other groups have suggested targeting ferroptosis (Gopal et al., 2023) and mTOR signaling (Dong et al., 2022). However, little has been published about the mechanistic underpinnings of why Complex I loss might be advantageous for tumor growth.

One line of inquiry to investigate this mechanism will be to characterize the metabolic changes engendered by Complex I loss in the setting of PTCs and ATCs by performing both targeted and untargeted metabolomics on TB vs TBN tumors. Our lab is also in the process of analyzing the metabolism of human TCV-PTC patient tumors and characterizing metabolic changes between TCV-PTC patients and classical PTC patients (data not shown). However, analysis of patient data from such experiments can prove convoluted due to inherent metabolic variability between tumors. Comparing human patient metabolomics with metabolomics from a more controlled mouse model like the TB/TBN model will be a valuable comparison to determine which underlying metabolic pathways might be the most important for the proliferation of Complex I-null thyroid tumors.

As *P53* loss is not a common feature of TCV-PTC (Jin et al., 2021; Malaguarnera et al., 2007; Olivier et al., 2002), the TBN model will also help to answer the question of whether thyroid-specific induction of the Braf V600E mutation and Complex I loss is sufficient to result in TCV-PTC. To do so, we plan to harvest TBN tumors and examine whether TBN tumors histologically resemble TCV-PTC; as TCV-PTC is clinically a diagnosis based on histology, H&E of TBN tumors is a reasonable readout for whether BrafV600E expression and Complex I loss is sufficient to induce TCV-PTC. If TBN tumors do in fact resemble TCV-PTC based on histology, the TBN model will also prove to be an invaluable tool to investigate the mechanism behind TCV-PTC development.

Finally, our mouse models will allow us to test the efficacy of novel therapeutics in Complex I-null thyroid tumors. MAPK inhibitors are already a widely prescribed treatment for PTC patients whose tumors are BRAF V600E positive (Fugazzola et al., 2019; Gild et al.,

2021). As our lab has already demonstrated that LDH inhibitors can halt the growth of 237 xenografts by exploiting a metabolic dependency of ETC deficiency, future experiments could also examine whether LDH inhibitors could be efficacious in the treatment of Complex I-null Braf V600E-driven thyroid malignancies using our murine model.

CHAPTER FIVE

Methodology

Animal studies

Animal studies were approved by the UT Southwestern Institutional Animal Care and Use Committee. Animals were given fresh diet pellets once per week.

Cell culture

Cell lines were maintained at 37°C with 5% CO_2. HEK 293T/17 were cultured in DMEM (Sigma D6429) supplemented with 10% FBS, 2 mM L-glutamine, 1% penicillin/streptomycin, and 50 μg/mL uridine. Cell lines were adapted to culture in HPLM supplemented with 2% FBS, 1% penicillin/streptomycin, and 1X insulin-transferrin-selenium for at least 5 passages. HPLM pool stocks were prepared and stored as previously described (Cantor et al., 2017) and HPLM was assembled by combining pool stock solutions in deionized water, adjusting pH to ~7.2 with hydrochloric acid, and filtering through a 0.22 μm PES filter. Prepared HPLM was used within 3-4 days and supplements were added daily before use. For cell growth assays removing individual metabolites, a separate pool solution that lacked the metabolite in question was prepared and used to prepare HPLM -pyruvate before pH adjustment and sterile filtration.

Lentivirus production

All lentiviruses were produced by co-transfection of HEK 293T/17 cells with plasmid DNA for the respective lentiviral vector and the packaging components psPAX2 and pMD2.G at a 5:3:2 mass ratio (vector:psPAX2:pMD2.G) using TransIT-LT1 (Mirus MIR 2300). Lentiviral

supernatants were collected at 48 and 72 hours post-transfection, pooled, and filtered using 0.45 μm PES filters before immediate use or aliquoting and storage at -80°C.

Targeted CRISPR-Cas9 screening

Genes were selected for targeted CRISPR-Cas9 screening based on the following criteria: i) the gene displayed ≥ 2-fold dropout in NCI-237 cells in the genome-wide screen; ii) the gene displayed ≥ 1.5-fold greater dropout in NCI-237 than TPC-1 in the genome-wide screen; iii) the gene was not depleted in > 99% of cell lines in The Cancer Dependency Map (www.depmap.org/portal/; DepMap Public 21Q2 Assembly) The targeted validation library sgRNA sequences were obtained from the Brunello library and synthesized as an oligo pool containing the sgRNA sequences with overhangs for Gibson assembly (Twist Biosciences). The sgRNA plasmid DNA library was constructed as described in (Joung et al., 2017) and sgRNA distribution in the library was assessed by next-generation sequencing. Cell lines conditioned to culture in HPLM or RPMI were infected with lentiCas9-Blast to generate cell lines stably expressing Cas9. Lentiviral titers were determined by selecting transduced cells with and without antibiotic. Cell counts were determined using a Vi-CELL (Beckman-Coulter). CRISPR-Cas9 screens and cell lines were infected in duplicate (approximately 8 x 10^6 cells per replicate) to achieve at least 1,000X cell coverage of the sgRNA library after puromycin selection. Cells were selected with puromycin as above before collecting an initial cell population (approximately 8 x 10^6 cells per replicate). Approximately 2 x 10^6 cells were maintained at each passage and cells were grown for approximately 14 population doublings before a final cell population was collected**.** Genomic DNA was purified using the Quick-DNA Miniprep Kit (Zymo Research D3024) and approximately 12 μg of genomic DNA was used

as a template for sgRNA cassette amplification as described above. PCR product purification, sequencing, and screen analysis were performed as for the genome-wide CRISPR-Cas9 screens. Depletion Scores were calculated as the (NCI-237 gene $\log_2$ fold-change) – (TPC-1 or UTSW-354 gene $\log_2$ fold-change).

***In vivo* CRISPR screening**

Custom *in vivo* screening library was designed and ordered from Twist Biosciences. 237 lentiCas9 blast cells were transduced with lentivirus containing the custom library cloned into lentiGuide-puro at MOI ~0.3 and selected with puromycin for seven days. At the end of the seven days, 237 Cas9 cells with the library were resuspended and mixed 1:1 with Geltrex (Thermo Fisher A1413202) at a final concentration of 20 x 10^6 cells/ml. NOD-SCID mice were anesthetized with isoflurane and xenografts were injected subcutaneously. Each xenograft consisted of 2 x 10^6 cells in a final volume of 100 µl.

Histology and immunohistochemistry

NCI-237-R xenograft fragments were fixed in 4% paraformaldehyde and incubated at 4°C for 24 hours with gentle shaking. Fixed lung adenocarcinomas were submitted to the UT Southwestern Histo Pathology Core for paraffin embedding and sectioning. Hematoxylin- and eosin-staining was performed by the UT Southwestern Histo Pathology Core. Fixed thyroid tumors and rhabdomyosarcomas were submitted to the UT Southwestern Tissue Management Shared Resource Core. Immunohistochemical staining was performed by the UT Southwestern Simmons Comprehensive Cancer Center Tissue Management Shared Resource using a Dako stainer. Whole-slide scans were captured at 40X magnification using a Nanozoomer

(Hamamatsu Photonics) and images were generated using QuPath software. Whole-slide scanning was performed at the UT Southwestern Whole Brain Microscopy Core.

Immunoblotting

For cell culture samples, media was removed, cells were washed 1 time with ice-cold PBS, and cells were lysed using Buffer A (50 mM HEPES pH 7.4, 10 mM KCl, 2 mM $MgCl_2$) with 1% SDS and 1:1,000 Benzonase® nuclease (Sigma E1014). Protein concentration was measured using A_{280} values determined by Cytation 5 (BioTek). Lysates were normalized in Buffer A with 1% SDS and prepared with 6X Laemmli sample buffer containing 100 mM 2-mercaptoethanol (Sigma M6250). Lysates were separated on 4-12% Bolt™ Bis-Tris gels (Invitrogen) using MES-SDS running buffer (Invitrogen B0002) and transferred to PVDF membranes using standard Towbin transfer buffer. After transfer, membranes were stained with 0.1% Ponceau S and stained membrane pictures were captured with a camera. Membranes were rinsed with TBS-0.1% Tween-20 (TBS-T) and blocked with 5% non-fat dry milk in TBS-T for 1 hour at room temperature. Membranes were rinsed with TBS-T 3 and incubated with primary antibodies overnight at 4°C. The following day, membranes were rinsed with TBS-T and incubated with secondary antibodies for 40 minutes at room temperature. Membranes were rinsed with TBS-T, incubated with Clarity Western ECL Substrate (BioRad 1705061) or SuperSignal West Pico PLUS Chemiluminescent Substrate (Thermo Fisher 34577), and exposed to X-ray film. Primary antibodies were diluted in 5% bovine serum albumin/TBS-T.

Targeting of Msh2 with AID tag

1 million 518T2 cells were nucleofected with 1 μg pUC19-Msh2-AID-P2A-BSD and 1 μg PX330-sg5. After 72 hours, the cells were selected with 8.5 μg/ml blasticidin (Invivogen) for

seven days. At the end of selection, clones were picked and expanded. Clones were screened by genotyping and Western blotting.

LentiCRISPR competition assay

237 pZIP ^{FLAG}Ndi1 hygro cells were transduced with sgRNAs of interest cloned into lentiCRISPR mCherry. The cells were transduced at MOI ~0.3 and initial percentage of mCherry-positive cells were assessed using a Cytek Guava easyCyte benchtop flow cytometer at 72 hours post-transduction. At each timepoint of interest, cells were trypsinized and resuspended in 1 ml media. 200 µl was used for flow cytometry and 200 µl was re-plated back into a 12-well plate.

Harvesting of gDNA from in vivo screening

Snap-frozen tissue was pulverized on dry ice. The pulverized tissue was incubated in genomic DNA (gDNA) extraction buffer [10 mM Tris pH 8, 100 mM NaCl, 10 mM EDTA pH 8, 0.5% SDS, 400 µg/ml proteinase K (Thermo Fisher P2308)] overnight at 55ºC. The mixture was then diluted 1:1 with phenol-chloroform-isoamyl alcohol (25:24:1) (Thermo Fisher #77617) and centrifuged in a Phase Lock tube (Fisher Scientific #FP2302830). Then, chloroform (Sigma-Aldrich #C2432) was added 1:1 to the mixture and centrifuged again at room temperature.

Nuclei counting assay

237 HIST1H4C mClover or TPC-1 HIST1H4C mClover were plated at 1,000 cells/well and 2,000 cells/well respectively into 96-well black-walled plates. The plate was loaded onto a Cytation plate reader (Biotek). The Cytation took pictures in four quadrants of the well, drew masks around cell nuclei, and counted the number of nuclei per frame.

Generation of CRISPaint HIST1H4C-tagged cell lines

For TPC, we plated 400,000 cells into a 12-well plate and transfected cells with lipofectamine. For each well, we added 100 µl OptiMEM + 250 ng pX330 + 250 ng sgHIST frameshift + 500 ng sgHIST mClover puro. After 72 hours, we selected cells with 2 µg/ml puromycin. To improve GFP signal, remaining cells were FACS sorted for the 10% brightest population. For 237, 3 million 237 cells were plated into 25 ml of HPLM in 10 cm dishes. The next day, the media was changed (adding 30 ml HPLM) and cells were transfected using lipofectamine. Cells were transfected with a total of 1.5 ml OptiMEM and 15 µg of DNA (3.75 µg PX330 + 3.75 µg sgframe + 7.5 µg HISTmClover donor). After 72 hours, we selected cells with 2 µg/ml puromycin. We validated the knock-in by observing cells under a fluorescent microscope for fluorescently-tagged nuclei.

Induction of thyroid tumors

20 mg/ml tamoxifen (MedChemExpress HY-13757A) was dissolved overnight at 37^{o}C in corn oil (Sigma C8267) protected from light while on a mini-rotator. Thyroid tumor induction was achieved by intraperitoneal tamoxifen injection of mice 8-12 weeks of age. Mice received 100 µl of 20 mg/ml tamoxifen on 2 consecutive days.

Infection with intratracheal adenoviral Cre

Ad5CMVCre (U of Iowa, VVC-U of Iowa-5) was thawed on wet ice and diluted in OptimEM (Life Technologies 319-85-062) to 1 x 10^5 PFU/µl. The adenovirus was precipitated with a final concentration of sterile-filtered 10mM $CaCl_2$ and incubated at room temperature for 20 minutes. Then, the adenovirus was placed on wet ice and used within 2

hours of receipt. Mice were anesthetized by ketamine/xylazine and each mouse received 50 μl of prepared adenovirus intratracheally, resulting in a dose of 5 x 10^6 PFU per mouse.

Infection with intramuscular adenoviral Cre

Ad5CMVCre (U of Iowa, VVC-U of Iowa-5) was thawed on wet ice and diluted in OptimEM (Life Technologies 319-85-062) to 2 x 10^4 PFU/μl. The adenovirus was precipitated with 10 mM sterile-filtered $CaCl_2$ and incubated at room temperature for 20 minutes. Then, the adenovirus was placed on wet ice and used within 2 hours of preparation. Mice were anesthetized by isoflurane and 500 μl of prepared adenovirus was injected into the mouse's left thigh, resulting in each mouse receiving 1 x 10^7 PFU of adenovirus.

APPENDIX A
List of reagents

Reagents: plasmids, DNA oligos, and antibodies

Plasmids

Name	Purpose	Source
pUC19-Msh2-AID-P2A-BSD	Transient expression of Msh2-AID-P2A-BSD repair template	This study
lentiCRISPR-mCherry	Lentiviral expression of Cas9 and mCherry fluorescent protein	This study
pZIP-FLAGNdi1-Hygro	Doxycycline-inducible expression of Ndi1 (internal FLAG) and hygromycin resistance	This study
lentiCas9-Blast	Lentiviral expression of Cas9	Feng Zhang, Addgene #52962
lentiGuide-Puro Brunello library	Lentiviral expression of genome-wide sgRNA library	Tiana Nguyen, Nijhawan lab; David Root and John Doench, Addgene #73178
lentiGuide-Puro Targeted validation library	Lentiviral expression of custom sgRNA library for validation of genome-wide screening hits	This study
sgHist-Frameshift +1	Lentiviral expression of LDHA	Veit Hornung, Addgene #66940
sgHIST-mClover-Puro	Lentiviral expression of $LDHA^{I141T}$	Veit Hornung, Addgene #80970
pX330-sgEmpty	Transient expression of Cas9 and non-targeting sgRNA	Feng Zhang, Addgene #42230
lentiGuide-Puro	Lentiviral expression of sgRNA	Feng Zhang, Addgene #52963
psPAX2	Lentiviral packaging plasmid	Didier Trono, Addgene #12260
pMD2.G	Lentiviral packaging plasmid	Didier Trono, Addgene #12259

DNA oligonucleotides

Name	Sequence (5' – 3')	Purpose
Msh2_C-term_sg5.Fw	CAC CGC ATT TCA CGG ATA AAG GCT C	sgRNA targeting *Msh2*
Msh2_C-term_sg5.Rv	AAA CGA GCC TTT ATC CGT GAA ATG C	sgRNA targeting *Msh2*

P5 0 nt stagger	AATGATACGGCGACCACCGAGATCT ACACTCTTTCCCTACACGACGCTCTT CCGATCTTTGTGGAAAGGACGAAAC ACCG	Amplification of sgRNA cassette from lentiGuide-Puro for NGS
P5 1nt stagger	AATGATACGGCGACCACCGAGATCT ACACTCTTTCCCTACACGACGCTCTT CCGATCTCTTGTGGAAAGGACGAAA CACCG	Amplification of sgRNA cassette from lentiGuide-Puro for NGS
P5 2 nt stagger	AATGATACGGCGACCACCGAGATCT ACACTCTTTCCCTACACGACGCTCTT CCGATCTGCTTGTGGAAAGGACGAA ACACCG	Amplification of sgRNA cassette from lentiGuide-Puro for NGS
P5 3 nt stagger	AATGATACGGCGACCACCGAGATCT ACACTCTTTCCCTACACGACGCTCTT CCGATCTAGCTTGTGGAAAGGACGA AACACCG	Amplification of sgRNA cassette from lentiGuide-Puro for NGS
P5 4 nt stagger	AATGATACGGCGACCACCGAGATCT ACACTCTTTCCCTACACGACGCTCTT CCGATCTCAACTTGTGGAAAGGACG AAACACCG	Amplification of sgRNA cassette from lentiGuide-Puro for NGS
P5 6 nt stagger	AATGATACGGCGACCACCGAGATCT ACACTCTTTCCCTACACGACGCTCTT CCGATCTTGCACCTTGTGGAAAGGA CGAAACACCG	Amplification of sgRNA cassette from lentiGuide-Puro for NGS
P5 7nt stagger	AATGATACGGCGACCACCGAGATCT ACACTCTTTCCCTACACGACGCTCTT CCGATCTACGCAACTTGTGGAAAGG ACGAAACACCG	Amplification of sgRNA cassette from lentiGuide-Puro for NGS
P5 8nt stagger	AATGATACGGCGACCACCGAGATCT ACACTCTTTCCCTACACGACGCTCTT CCGATCTGAAGACCCTTGTGGAAAG GACGAAACACCG	Amplification of sgRNA cassette from lentiGuide-Puro for NGS
P7 lentiGuide A1	CAAGCAGAAGACGGCATACGAGATC GGTTCAAGTGACTGGAGTTCAGACG TGTGCTCTTCCGATCTTCTACTATTCT TTCCCCTGCACTGT	Amplification of sgRNA cassette from lentiGuide-Puro for NGS
P7 lentiGuide A3	CAAGCAGAAGACGGCATACGAGATT AACTCGGGTGACTGGAGTTCAGACG TGTGCTCTTCCGATCTTCTACTATTCT TTCCCCTGCACTGT	Amplification of sgRNA cassette from lentiGuide-Puro for NGS
P7 lentiGuide A5	CAAGCAGAAGACGGCATACGAGATA TACTCAAGTGACTGGAGTTCAGACG	Amplification of sgRNA cassette

	TGTGCTCTTCCGATCTTCTACTATTCT TTCCCCTGCACTGT	from lentiGuide-Puro for NGS
P7 lentiGuide A6	CAAGCAGAAGACGGCATACGAGATG CTGAGAAGTGACTGGAGTTCAGACG TGTGCTCTTCCGATCTTCTACTATTCT TTCCCCTGCACTGT	Amplification of sgRNA cassette from lentiGuide-Puro for NGS
P7 lentiGuide B1	CAAGCAGAAGACGGCATACGAGATA TTGGATTGTGACTGGAGTTCAGACGT GTGCTCTTCCGATCTTCTACTATTCTT TCCCCTGCACTGT	Amplification of sgRNA cassette from lentiGuide-Puro for NGS
P7 lentiGuide B3	CAAGCAGAAGACGGCATACGAGATT ATGAGAAGTGACTGGAGTTCAGACG TGTGCTCTTCCGATCTTCTACTATTCT TTCCCCTGCACTGT	Amplification of sgRNA cassette from lentiGuide-Puro for NGS
P7 lentiGuide B7	CAAGCAGAAGACGGCATACGAGATG CACGATTGTGACTGGAGTTCAGACG TGTGCTCTTCCGATCTTCTACTATTCT TTCCCCTGCACTGT	Amplification of sgRNA cassette from lentiGuide-Puro for NGS
P7 lentiGuide B12	CAAGCAGAAGACGGCATACGAGATC GCATCAAGTGACTGGAGTTCAGACG TGTGCTCTTCCGATCTTCTACTATTCT TTCCCCTGCACTGT	Amplification of sgRNA cassette from lentiGuide-Puro for NGS
P7 lentiGuide C1	CAAGCAGAAGACGGCATACGAGATG CACGACCGTGACTGGAGTTCAGACG TGTGCTCTTCCGATCTTCTACTATTCT TTCCCCTGCACTGT	Amplification of sgRNA cassette from lentiGuide-Puro for NGS
P7 lentiGuide C4	CAAGCAGAAGACGGCATACGAGATA TGTTCGGGTGACTGGAGTTCAGACG TGTGCTCTTCCGATCTTCTACTATTCT TTCCCCTGCACTGT	Amplification of sgRNA cassette from lentiGuide-Puro for NGS
P7 lentiGuide C5	CAAGCAGAAGACGGCATACGAGATC GTGGACCGTGACTGGAGTTCAGACG TGTGCTCTTCCGATCTTCTACTATTCT TTCCCCTGCACTGT	Amplification of sgRNA cassette from lentiGuide-Puro for NGS
P7 lentiGuide C6	CAAGCAGAAGACGGCATACGAGATA TTGAGCCGTGACTGGAGTTCAGACG TGTGCTCTTCCGATCTTCTACTATTCT TTCCCCTGCACTGT	Amplification of sgRNA cassette from lentiGuide-Puro for NGS
P7 lentiGuide E1	CAAGCAGAAGACGGCATACGAGATT AACTCAAGTGACTGGAGTTCAGACG TGTGCTCTTCCGATCTTCTACTATTCT TTCCCCTGCACTGT	Amplification of sgRNA cassette from lentiGuide-Puro for NGS

P7 lentiGuide E2	CAAGCAGAAGACGGCATACGAGATC GTGAGCCGTGACTGGAGTTCAGACG TGTGCTCTTCCGATCTTCTACTATTCT TTCCCCTGCACTGT	Amplification of sgRNA cassette from lentiGuide-Puro for NGS
P7 lentiGuide E3	CAAGCAGAAGACGGCATACGAGATA TCAGAGGGTGACTGGAGTTCAGACG TGTGCTCTTCCGATCTTCTACTATTCT TTCCCCTGCACTGT	Amplification of sgRNA cassette from lentiGuide-Puro for NGS
P7 lentiGuide E5	CAAGCAGAAGACGGCATACGAGATG CGTTCAAGTGACTGGAGTTCAGACG TGTGCTCTTCCGATCTTCTACTATTCT TTCCCCTGCACTGT	Amplification of sgRNA cassette from lentiGuide-Puro for NGS
P7 lentiGuide F1	CAAGCAGAAGACGGCATACGAGATA TGTTCTTGTGACTGGAGTTCAGACGT GTGCTCTTCCGATCTTCTACTATTCTT TCCCCTGCACTGT	Amplification of sgRNA cassette from lentiGuide-Puro for NGS
P7 lentiGuide F3	CAAGCAGAAGACGGCATACGAGATG CACTCAAGTGACTGGAGTTCAGACG TGTGCTCTTCCGATCTTCTACTATTCT TTCCCCTGCACTGT	Amplification of sgRNA cassette from lentiGuide-Puro for NGS
P7 lentiGuide F4	CAAGCAGAAGACGGCATACGAGATT AGTAGCCGTGACTGGAGTTCAGACG TGTGCTCTTCCGATCTTCTACTATTCT TTCCCCTGCACTGT	Amplification of sgRNA cassette from lentiGuide-Puro for NGS
P7 lentiGuide F5	CAAGCAGAAGACGGCATACGAGATC GTGTCAAGTGACTGGAGTTCAGACG TGTGCTCTTCCGATCTTCTACTATTCT TTCCCCTGCACTGT	Amplification of sgRNA cassette from lentiGuide-Puro for NGS
P7 lentiGuide G1	CAAGCAGAAGACGGCATACGAGATG CGTAGCCGTGACTGGAGTTCAGACG TGTGCTCTTCCGATCTTCTACTATTCT TTCCCCTGCACTGT	Amplification of sgRNA cassette from lentiGuide-Puro for NGS
P7 lentiGuide G2	CAAGCAGAAGACGGCATACGAGATC GACAGAAGTGACTGGAGTTCAGACG TGTGCTCTTCCGATCTTCTACTATTCT TTCCCCTGCACTGT	Amplification of sgRNA cassette from lentiGuide-Puro for NGS
P7 lentiGuide G3	CAAGCAGAAGACGGCATACGAGATT AGTCTGGGTGACTGGAGTTCAGACG TGTGCTCTTCCGATCTTCTACTATTCT TTCCCCTGCACTGT	Amplification of sgRNA cassette from lentiGuide-Puro for NGS
P7 lentiGuide G6	CAAGCAGAAGACGGCATACGAGATA TACTCTTGTGACTGGAGTTCAGACGT	Amplification of sgRNA cassette

	GTGCTCTTCCGATCTTCTACTATTCTTTCCCCTGCACTGT	from lentiGuide-Puro for NGS
lentiGuide_library_clone_F	GTAACTTGAAAGTATTTCGATTTCTTGGCTTTATATATCTTGTGGAAAGGACGAAACACC	Gibson cloning sgRNA cassette into lentiGuide-Puro for custom sgRNA library
lentiGuide_library_clone_R	ACTTTTTCAAGTTGATAACGGACTAGCCTTATTTTAACTTGCTATTTCTAGCTCTAAAAC	Gibson cloning sgRNA cassette into lentiGuide-Puro for custom sgRNA library
RPS27_sg1.Fw	CACCGTTGTGCATGGCTAAAGACCG	sgRNA targeting RPS27 with overhangs to be cloned into lentiCRISPR mCherry
RPS27_sg1.Rv	AAACCGGTCTTTAGCCATGCACAAC	sgRNA targeting *RPS27* with overhangs to be cloned into lentiCRISPR mCherry
RPS27_sg2.Fw	CACCGTTCATGGATGTGAAATGCCC	sgRNA targeting *RPS27* with overhangs to be cloned into lentiCRISPR mCherry
RPS27_sg2.Rv	AAACGGGCATTTCACATCCATGAAC	sgRNA targeting *RPS27* with overhangs to be cloned into lentiCRISPR mCherry
RPSA_sg1.Fw	CACCGCATAAATCTCAAGAGGACCT	sgRNA targeting *RPSA* with overhangs to be cloned into lentiCRISPR mCherry

RPSA_sg1.Rv	AAACAGGTCCTCTTGAGATTTATGC	sgRNA targeting *RPSA* with overhangs to be cloned into lentiCRISPR mCherry
RPSA_sg2.Fw	CACCGTACACAGCGCAATGGTAGGT	sgRNA targeting *RPSA* with overhangs to be cloned into lentiCRISPR mCherry
RPSA_sg2.Rv	AAACACCTACCATTGCGCTGTGTAC	sgRNA targeting *RPSA* with overhangs to be cloned into lentiCRISPR mCherry
ZBTB8OS_sg1.Fw	CACCGTGAAGAACAGAAGGCGATCA	sgRNA targeting *ZBTB8OS* with overhangs to be cloned into lentiCRISPR mCherry
ZBTB8OS_sg1.Rv	AAACTGATCGCCTTCTGTTCTTCAC	sgRNA targeting *ZBTB8OS* with overhangs to be cloned into lentiCRISPR mCherry
ZBTB8OS_sg2.Fw	CACCGTCTACTTCTACTGTTTGGAG	sgRNA targeting *ZBTB8OS* with overhangs to be cloned into lentiCRISPR mCherry
ZBTB8OS_sg2.Rv	AAACCTCCAAACAGTAGAAGTAGAC	sgRNA targeting *ZBTB8OS* with overhangs to be cloned into lentiCRISPR mCherry
MVD_sg1.Fw	CACCGAAGCTGACAGGCAGTACCGT	sgRNA targeting *MVD* with

		overhangs to be cloned into lentiCRISPR mCherry
MVD_sg1.Rv	AAACACGGTACTGCCTGTCAGCTTC	sgRNA targeting *MVD* with overhangs to be cloned into lentiCRISPR mCherry
MVD_sg2.Fw	CACCGCTGGTGCAGAGTGACGCTCA	sgRNA targeting *MVD* with overhangs to be cloned into lentiCRISPR mCherry
MVD_sg2.Rv	AAACTGAGCGTCACTCTGCACCAGC	sgRNA targeting *MVD* with overhangs to be cloned into lentiCRISPR mCherry
PSMG3_sg1.Fw	CACCGTCACCACAAAAGTCCTTCTG	sgRNA targeting *PSMG3* with overhangs to be cloned into lentiCRISPR mCherry
PSMG3_sg1.Rv	AAACCAGAAGGACTTTTGTGGTGAC	sgRNA targeting *PSMG3* with overhangs to be cloned into lentiCRISPR mCherry
PSMG3_sg2.Fw	CACCGGTGACCCAGTTTGGGAAGAT	sgRNA targeting *PSMG3* with overhangs to be cloned into lentiCRISPR mCherry
PSMG3_sg2.Rv	AAACATCTTCCCAAACTGGGTCACC	sgRNA targeting *PSMG3* with overhangs to be cloned into

		lentiCRISPR mCherry
ATP5D_sg1.Fw	CACCGCAACAACTGCACCGAAGAGT	sgRNA targeting *ATP5D* with overhangs to be cloned into lentiCRISPR mCherry
ATP5D_sg1.Rv	AAACACTCTTCGGTGCAGTTGTTGC	sgRNA targeting *ATP5D* with overhangs to be cloned into lentiCRISPR mCherry
ATP5D_sg2.Fw	CACCGCCCATTCCCCCAGTGAGCAG	sgRNA targeting *ATP5D* with overhangs to be cloned into lentiCRISPR mCherry
ATP5D_sg2.Rv	AAACCTGCTCACTGGGGGAATGGGC	sgRNA targeting *ATP5D* with overhangs to be cloned into lentiCRISPR mCherry
GPI_sg1.Fw	CACCGTGGGAGGACGCTACTCGCTG	sgRNA targeting *GPI* with overhangs to be cloned into lentiCRISPR mCherry
GPI_sg1.Rv	AAACCAGCGAGTAGCGTCCTCCCAC	sgRNA targeting *GPI* with overhangs to be cloned into lentiCRISPR mCherry
GPI_sg2.Fw	CACCGTGAGAAGATCAACTACACCG	sgRNA targeting *GPI* with overhangs to be cloned into lentiCRISPR mCherry
GPI_sg2.Rv	AAACCGGTGTAGTTGATCTTCTCAC	sgRNA targeting *GPI* with overhangs

		to be cloned into lentiCRISPR mCherry

Antibodies

Name	Catalog Number	Application	Dilution
anti-MSH2	Cell Signaling #2017	WB	1:2,000
anti-α tubulin	Cell Signaling #3873S	WB	1:1,000
anti-HSP90	BD Biosciences #610418	WB	1:2,000
anti-NDUFS4	Abcam #ab137064	IHC-P	1:200
anti-Prohibitin	Abcam #ab28172	IHC-P	1 μg/ml
anti-Ndufa9	Thermo Fisher #459100	WB	1:1,000

BIBLIOGRAPHY

Albain, K. S., Crowley, J. J., & Livingston, R. B. (1991). Long-term survival and toxicity in small cell lung cancer. Expanded Southwest Oncology Group experience. *Chest*, *99*(6), 1425-1432. https://doi.org/10.1378/chest.99.6.1425

Anderson, S., Bankier, A. T., Barrell, B. G., de Bruijn, M. H., Coulson, A. R., Drouin, J., Eperon, I. C., Nierlich, D. P., Roe, B. A., Sanger, F., Schreier, P. H., Smith, A. J., Staden, R., & Young, I. G. (1981). Sequence and organization of the human mitochondrial genome. *Nature*, *290*(5806), 457-465. https://doi.org/10.1038/290457a0

Bartman, C. R., Weilandt, D. R., Shen, Y., Lee, W. D., Han, Y., TeSlaa, T., Jankowski, C. S. R., Samarah, L., Park, N. R., da Silva-Diz, V., Aleksandrova, M., Gultekin, Y., Marishta, A., Wang, L., Yang, L., Roichman, A., Bhatt, V., Lan, T., Hu, Z., . . . Rabinowitz, J. D. (2023). Slow TCA flux and ATP production in primary solid tumours but not metastases. *Nature*, *614*(7947), 349-357. https://doi.org/10.1038/s41586-022-05661-6

Berthold, J., Bauer, M. F., Schneider, H. C., Klaus, C., Dietmeier, K., Neupert, W., & Brunner, M. (1995). The MIM complex mediates preprotein translocation across the mitochondrial inner membrane and couples it to the mt-Hsp70/ATP driving system. *Cell*, *81*(7), 1085-1093. https://doi.org/10.1016/s0092-8674(05)80013-3

Bhattacharyya, N. (2003). Survival and prognosis in Hurthle cell carcinoma of the thyroid gland. *Arch Otolaryngol Head Neck Surg*, *129*(2), 207-210. https://doi.org/10.1001/archotol.129.2.207

Birsoy, K., Wang, T., Chen, W. W., Freinkman, E., Abu-Remaileh, M., & Sabatini, D. M. (2015). An Essential Role of the Mitochondrial Electron Transport Chain in Cell Proliferation Is to Enable Aspartate Synthesis. *Cell*, *162*(3), 540-551. https://doi.org/10.1016/j.cell.2015.07.016

Bonora, E., Porcelli, A. M., Gasparre, G., Biondi, A., Ghelli, A., Carelli, V., Baracca, A., Tallini, G., Martinuzzi, A., Lenaz, G., Rugolo, M., & Romeo, G. (2006). Defective oxidative phosphorylation in thyroid oncocytic carcinoma is associated with pathogenic mitochondrial DNA mutations affecting complexes I and III. *Cancer Res*, *66*(12), 6087-6096. https://doi.org/10.1158/0008-5472.CAN-06-0171

Budde, S. M., van den Heuvel, L. P., Smeets, R. J., Skladal, D., Mayr, J. A., Boelen, C., Petruzzella, V., Papa, S., & Smeitink, J. A. (2003). Clinical heterogeneity in patients with mutations in the NDUFS4 gene of mitochondrial complex I. *J Inherit Metab Dis*, *26*(8), 813-815. https://doi.org/10.1023/b:boli.0000010003.14113.af

Cantor, J. R., Abu-Remaileh, M., Kanarek, N., Freinkman, E., Gao, X., Louissaint, A., Jr., Lewis, C. A., & Sabatini, D. M. (2017). Physiologic Medium Rewires Cellular Metabolism and Reveals Uric Acid as an Endogenous Inhibitor of UMP Synthase. *Cell*, *169*(2), 258-272 e217. https://doi.org/10.1016/j.cell.2017.03.023

Cantwell-Dorris, E. R., O'Leary, J. J., & Sheils, O. M. (2011). BRAFV600E: implications for carcinogenesis and molecular therapy. *Mol Cancer Ther*, *10*(3), 385-394. https://doi.org/10.1158/1535-7163.MCT-10-0799

Cargnello, M., & Roux, P. P. (2011). Activation and function of the MAPKs and their substrates, the MAPK-activated protein kinases. *Microbiol Mol Biol Rev*, *75*(1), 50-83. https://doi.org/10.1128/MMBR.00031-10

Castoreno, A. B., Smurnyy, Y., Torres, A. D., Vokes, M. S., Jones, T. R., Carpenter, A. E., & Eggert, U. S. (2010). Small molecules discovered in a pathway screen target the Rho pathway in cytokinesis. *Nat Chem Biol*, *6*(6), 457-463. https://doi.org/10.1038/nchembio.363

Chandel, N. S. (2021). Glycolysis. *Cold Spring Harb Perspect Biol*, *13*(5). https://doi.org/10.1101/cshperspect.a040535

Chung, H. K., Jacobs, C. L., Huo, Y., Yang, J., Krumm, S. A., Plemper, R. K., Tsien, R. Y., & Lin, M. Z. (2015). Tunable and reversible drug control of protein production via a self-excising degron. *Nat Chem Biol*, *11*(9), 713-720. https://doi.org/10.1038/nchembio.1869

Crofts, A. R., Hong, S., Wilson, C., Burton, R., Victoria, D., Harrison, C., & Schulten, K. (2013). The mechanism of ubihydroquinone oxidation at the Qo-site of the cytochrome bc1 complex. *Biochim Biophys Acta*, *1827*(11-12), 1362-1377. https://doi.org/10.1016/j.bbabio.2013.01.009

Dong, Y., Gong, Y., Kuo, F., Makarov, V., Reznik, E., Nanjangud, G. J., Aras, O., Zhao, H., Qu, R., Fagin, J. A., Sherman, E. J., Xu, B., Ghossein, R., Chan, T. A., & Ganly, I. (2022). Targeting the mTOR Pathway in Hurthle Cell Carcinoma Results in Potent Antitumor Activity. *Mol Cancer Ther*, *21*(2), 382-394. https://doi.org/10.1158/1535-7163.MCT-21-0224

Feldman, P. S., Horvath, E., & Kovacs, K. (1972). Ultrastructure of three Hurthle cell tumors of the thyroid. *Cancer*, *30*(5), 1279-1285. https://doi.org/10.1002/1097-0142(197211)30:5<1279::aid-cncr2820300521>3.0.co;2-q

Frank, A. R., Li, V., Shelton, S. D., Kim, J., Stott, G. M., Neckers, L. M., Xie, Y., Williams, N. S., Mishra, P., & McFadden, D. G. (2023). Mitochondrial-Encoded Complex I Impairment Induces a Targetable Dependency on Aerobic Fermentation in Hurthle Cell Carcinoma of the Thyroid. *Cancer Discov*, *13*(8), 1884-1903. https://doi.org/10.1158/2159-8290.CD-22-0982

Frank, A. R., Vandiver, F., & McFadden, D. G. (2024). Forward Genetic Screens Identify Mechanisms of Resistance to Small-Molecule Lactate Dehydrogenase Inhibitors. *ACS Chem Biol*, *19*(2), 471-482. https://doi.org/10.1021/acschembio.3c00663

Fugazzola, L., Elisei, R., Fuhrer, D., Jarzab, B., Leboulleux, S., Newbold, K., & Smit, J. (2019). 2019 European Thyroid Association Guidelines for the Treatment and Follow-Up of Advanced Radioiodine-Refractory Thyroid Cancer. *Eur Thyroid J*, *8*(5), 227-245. https://doi.org/10.1159/000502229

Ganly, I., Makarov, V., Deraje, S., Dong, Y., Reznik, E., Seshan, V., Nanjangud, G., Eng, S., Bose, P., Kuo, F., Morris, L. G. T., Landa, I., Carrillo Albornoz, P. B., Riaz, N., Nikiforov, Y. E., Patel, K., Umbricht, C., Zeiger, M., Kebebew, E., . . . Chan, T. A. (2018). Integrated Genomic Analysis of Hurthle Cell Cancer Reveals Oncogenic Drivers, Recurrent Mitochondrial Mutations, and Unique Chromosomal Landscapes. *Cancer Cell*, *34*(2), 256-270 e255. https://doi.org/10.1016/j.ccell.2018.07.002

Gasparre, G., Porcelli, A. M., Bonora, E., Pennisi, L. F., Toller, M., Iommarini, L., Ghelli, A., Moretti, M., Betts, C. M., Martinelli, G. N., Ceroni, A. R., Curcio, F., Carelli, V., Rugolo, M., Tallini, G., & Romeo, G. (2007). Disruptive mitochondrial DNA mutations in complex I subunits are markers of oncocytic phenotype in thyroid tumors. *Proc Natl Acad Sci U S A*, *104*(21), 9001-9006. https://doi.org/10.1073/pnas.0703056104

Gasparre, G., Romeo, G., Rugolo, M., & Porcelli, A. M. (2011). Learning from oncocytic tumors: Why choose inefficient mitochondria? *Biochim Biophys Acta*, *1807*(6), 633-642. https://doi.org/10.1016/j.bbabio.2010.08.006

Ghossein, R., & Livolsi, V. A. (2008). Papillary thyroid carcinoma tall cell variant. *Thyroid*, *18*(11), 1179-1181. https://doi.org/10.1089/thy.2008.0164

Gild, M. L., Tsang, V. H. M., Clifton-Bligh, R. J., & Robinson, B. G. (2021). Multikinase inhibitors in thyroid cancer: timing of targeted therapy. *Nat Rev Endocrinol*, *17*(4), 225-234. https://doi.org/10.1038/s41574-020-00465-y

Gopal, R. K., Calvo, S. E., Shih, A. R., Chaves, F. L., McGuone, D., Mick, E., Pierce, K. A., Li, Y., Garofalo, A., Van Allen, E. M., Clish, C. B., Oliva, E., & Mootha, V. K. (2018). Early loss of mitochondrial complex I and rewiring of glutathione metabolism in renal oncocytoma. *Proc Natl Acad Sci U S A*, *115*(27), E6283-E6290. https://doi.org/10.1073/pnas.1711888115

Gopal, R. K., Kubler, K., Calvo, S. E., Polak, P., Livitz, D., Rosebrock, D., Sadow, P. M., Campbell, B., Donovan, S. E., Amin, S., Gigliotti, B. J., Grabarek, Z., Hess, J. M., Stewart, C., Braunstein, L. Z., Arndt, P. F., Mordecai, S., Shih, A. R., Chaves, F., . . . McFadden, D. G. (2018). Widespread Chromosomal Losses and Mitochondrial DNA Alterations as Genetic Drivers in Hurthle Cell Carcinoma. *Cancer Cell*, *34*(2), 242-255 e245. https://doi.org/10.1016/j.ccell.2018.06.013

Gopal, R. K., Vantaku, V. R., Panda, A., Reimer, B., Rath, S., To, T. L., Fisch, A. S., Cetinbas, M., Livneh, M., Calcaterra, M. J., Gigliotti, B. J., Pierce, K. A., Clish, C. B., Dias-Santagata, D., Sadow, P. M., Wirth, L. J., Daniels, G. H., Sadreyev, R. I., Calvo, S. E., . . . Mootha, V. K. (2023). Effectors Enabling Adaptation to Mitochondrial Complex I Loss in Hurthle Cell Carcinoma. *Cancer Discov*, *13*(8), 1904-1921. https://doi.org/10.1158/2159-8290.CD-22-0976

Gorelick, A. N., Kim, M., Chatila, W. K., La, K., Hakimi, A. A., Berger, M. F., Taylor, B. S., Gammage, P. A., & Reznik, E. (2021). Respiratory complex and tissue lineage drive recurrent mutations in tumour mtDNA. *Nat Metab*, *3*(4), 558-570. https://doi.org/10.1038/s42255-021-00378-8

Gray, W. M., del Pozo, J. C., Walker, L., Hobbie, L., Risseeuw, E., Banks, T., Crosby, W. L., Yang, M., Ma, H., & Estelle, M. (1999). Identification of an SCF ubiquitin-ligase complex required for auxin response in Arabidopsis thaliana. *Genes Dev*, *13*(13), 1678-1691. https://doi.org/10.1101/gad.13.13.1678

Gray, W. M., Kepinski, S., Rouse, D., Leyser, O., & Estelle, M. (2001). Auxin regulates SCF(TIR1)-dependent degradation of AUX/IAA proteins. *Nature*, *414*(6861), 271-276. https://doi.org/10.1038/35104500

Han, T., Goralski, M., Capota, E., Padrick, S. B., Kim, J., Xie, Y., & Nijhawan, D. (2016). The antitumor toxin CD437 is a direct inhibitor of DNA polymerase alpha. *Nat Chem Biol*, *12*(7), 511-515. https://doi.org/10.1038/nchembio.2082

Han, T., Goralski, M., Gaskill, N., Capota, E., Kim, J., Ting, T. C., Xie, Y., Williams, N. S., & Nijhawan, D. (2017). Anticancer sulfonamides target splicing by inducing RBM39 degradation via recruitment to DCAF15. *Science*, *356*(6336). https://doi.org/10.1126/science.aal3755

Helin, K., Holm, K., Niebuhr, A., Eiberg, H., Tommerup, N., Hougaard, S., Poulsen, H. S., Spang-Thomsen, M., & Norgaard, P. (1997). Loss of the retinoblastoma protein-related p130 protein in small cell lung carcinoma. *Proc Natl Acad Sci U S A*, *94*(13), 6933-6938. https://doi.org/10.1073/pnas.94.13.6933

Hensley, C. T., Faubert, B., Yuan, Q., Lev-Cohain, N., Jin, E., Kim, J., Jiang, L., Ko, B., Skelton, R., Loudat, L., Wodzak, M., Klimko, C., McMillan, E., Butt, Y., Ni, M., Oliver, D., Torrealba, J., Malloy, C. R., Kernstine, K., . . . DeBerardinis, R. J. (2016). Metabolic Heterogeneity in Human Lung Tumors. *Cell*, *164*(4), 681-694. https://doi.org/10.1016/j.cell.2015.12.034

Hunt, J. L., Tometsko, M., LiVolsi, V. A., Swalsky, P., Finkelstein, S. D., & Barnes, E. L. (2003). Molecular evidence of anaplastic transformation in coexisting well-differentiated and anaplastic carcinomas of the thyroid. *Am J Surg Pathol*, *27*(12), 1559-1564. https://doi.org/10.1097/00000478-200312000-00009

Ito, Y., Miyauchi, A., Kihara, M., Fukushima, M., Higashiyama, T., & Miya, A. (2018). Overall Survival of Papillary Thyroid Carcinoma Patients: A Single-Institution Long-Term Follow-Up of 5897 Patients. *World J Surg*, *42*(3), 615-622. https://doi.org/10.1007/s00268-018-4479-z

Jin, M., Song, D. E., Ahn, J., Song, E., Lee, Y. M., Sung, T. Y., Kim, T. Y., Kim, W. B., Shong, Y. K., Jeon, M. J., & Kim, W. G. (2021). Genetic Profiles of Aggressive Variants of Papillary Thyroid Carcinomas. *Cancers (Basel)*, *13*(4). https://doi.org/10.3390/cancers13040892

Jones, W., & Bianchi, K. (2015). Aerobic glycolysis: beyond proliferation. *Front Immunol*, *6*, 227. https://doi.org/10.3389/fimmu.2015.00227

Joost, H. G., & Thorens, B. (2001). The extended GLUT-family of sugar/polyol transport facilitators: nomenclature, sequence characteristics, and potential function of its novel members (review). *Mol Membr Biol*, *18*(4), 247-256. https://doi.org/10.1080/09687680110090456

Joshi, S., Tolkunov, D., Aviv, H., Hakimi, A. A., Yao, M., Hsieh, J. J., Ganesan, S., Chan, C. S., & White, E. (2015). The Genomic Landscape of Renal Oncocytoma Identifies a Metabolic Barrier to Tumorigenesis. *Cell Rep*, *13*(9), 1895-1908. https://doi.org/10.1016/j.celrep.2015.10.059

Joung, J., Konermann, S., Gootenberg, J. S., Abudayyeh, O. O., Platt, R. J., Brigham, M. D., Sanjana, N. E., & Zhang, F. (2017). Genome-scale CRISPR-Cas9 knockout and transcriptional activation screening. *Nat Protoc*, *12*(4), 828-863. https://doi.org/10.1038/nprot.2017.016

Ke, B. X., Pepe, S., Grubb, D. R., Komen, J. C., Laskowski, A., Rodda, F. A., Hardman, B. M., Pitt, J. J., Ryan, M. T., Lazarou, M., Koleff, J., Cheung, M. M., Smolich, J.

J., & Thorburn, D. R. (2012). Tissue-specific splicing of an Ndufs6 gene-trap insertion generates a mitochondrial complex I deficiency-specific cardiomyopathy. *Proc Natl Acad Sci U S A*, *109*(16), 6165-6170. https://doi.org/10.1073/pnas.1113987109

Khairy, G. (2009). Anaplastic transformation of differentiated thyroid carcinoma. *Int J Health Sci (Qassim)*, *3*(1), 93-96. https://www.ncbi.nlm.nih.gov/pubmed/21475516

Kiebler, M., Pfaller, R., Sollner, T., Griffiths, G., Horstmann, H., Pfanner, N., & Neupert, W. (1990). Identification of a mitochondrial receptor complex required for recognition and membrane insertion of precursor proteins. *Nature*, *348*(6302), 610-616. https://doi.org/10.1038/348610a0

King, M. P., & Attardi, G. (1989). Human cells lacking mtDNA: repopulation with exogenous mitochondria by complementation. *Science*, *246*(4929), 500-503. https://doi.org/10.1126/science.2814477

Kondo, T., Ezzat, S., & Asa, S. L. (2006). Pathogenetic mechanisms in thyroid follicular-cell neoplasia. *Nat Rev Cancer*, *6*(4), 292-306. https://doi.org/10.1038/nrc1836

Kotrys, A. V., Durham, T. J., Guo, X. A., Vantaku, V. R., Parangi, S., & Mootha, V. K. (2024). Single-cell analysis reveals context-dependent, cell-level selection of mtDNA. *Nature*, *629*(8011), 458-466. https://doi.org/10.1038/s41586-024-07332-0

Kruse, S. E., Watt, W. C., Marcinek, D. J., Kapur, R. P., Schenkman, K. A., & Palmiter, R. D. (2008). Mice with mitochondrial complex I deficiency develop a fatal encephalomyopathy. *Cell Metab*, *7*(4), 312-320. https://doi.org/10.1016/j.cmet.2008.02.004

Langhans, T. (1907). Über die epithelialen Formen der malignen Struma. *Virchows Arch (Pathol Anat)*, *189*, 69-152. https://doi.org/https://doi.org/10.1007/BF02176714

Lassen, U., Osterlind, K., Hansen, M., Dombernowsky, P., Bergman, B., & Hansen, H. H. (1995). Long-term survival in small-cell lung cancer: posttreatment characteristics in patients surviving 5 to 18+ years--an analysis of 1,714 consecutive patients. *J Clin Oncol*, *13*(5), 1215-1220. https://doi.org/10.1200/JCO.1995.13.5.1215

Lerman, L. S. (1953). A Biochemically Specific Method for Enzyme Isolation. *Proc Natl Acad Sci U S A*, *39*(4), 232-236. https://doi.org/10.1073/pnas.39.4.232

Lim, H., Devesa, S. S., Sosa, J. A., Check, D., & Kitahara, C. M. (2017). Trends in Thyroid Cancer Incidence and Mortality in the United States, 1974-2013. *JAMA*, *317*(13), 1338-1348. https://doi.org/10.1001/jama.2017.2719

Lloyd RV, O. R., Kloppel G, Rosai J. (2017). WHO classification of tumours: pathology and genetics of tumours of endocrine organs. IARC, Lyon.

Longheu, A., Canu, G. L., Cappellacci, F., Erdas, E., Medas, F., & Calo, P. G. (2020). Tall Cell Variant versus Conventional Papillary Thyroid Carcinoma: A Retrospective Analysis in 351 Consecutive Patients. *J Clin Med*, *10*(1). https://doi.org/10.3390/jcm10010070

Maher, E. A., Marin-Valencia, I., Bachoo, R. M., Mashimo, T., Raisanen, J., Hatanpaa, K. J., Jindal, A., Jeffrey, F. M., Choi, C., Madden, C., Mathews, D., Pascual, J.

M., Mickey, B. E., Malloy, C. R., & DeBerardinis, R. J. (2012). Metabolism of [U-13 C]glucose in human brain tumors in vivo. *NMR Biomed*, *25*(11), 1234-1244. https://doi.org/10.1002/nbm.2794

Malaguarnera, R., Vella, V., Vigneri, R., & Frasca, F. (2007). p53 family proteins in thyroid cancer. *Endocr Relat Cancer*, *14*(1), 43-60. https://doi.org/10.1677/erc.1.01223

Martinez-Reyes, I., Cardona, L. R., Kong, H., Vasan, K., McElroy, G. S., Werner, M., Kihshen, H., Reczek, C. R., Weinberg, S. E., Gao, P., Steinert, E. M., Piseaux, R., Budinger, G. R. S., & Chandel, N. S. (2020). Mitochondrial ubiquinol oxidation is necessary for tumour growth. *Nature*, *585*(7824), 288-292. https://doi.org/10.1038/s41586-020-2475-6

Maximo, V., Soares, P., Lima, J., Cameselle-Teijeiro, J., & Sobrinho-Simoes, M. (2002). Mitochondrial DNA somatic mutations (point mutations and large deletions) and mitochondrial DNA variants in human thyroid pathology: a study with emphasis on Hurthle cell tumors. *Am J Pathol*, *160*(5), 1857-1865. https://doi.org/10.1016/S0002-9440(10)61132-7

McFadden, D. G., Vernon, A., Santiago, P. M., Martinez-McFaline, R., Bhutkar, A., Crowley, D. M., McMahon, M., Sadow, P. M., & Jacks, T. (2014). p53 constrains progression to anaplastic thyroid carcinoma in a Braf-mutant mouse model of papillary thyroid cancer. *Proc Natl Acad Sci U S A*, *111*(16), E1600-1609. https://doi.org/10.1073/pnas.1404357111

Miller, C. W., Simon, K., Aslo, A., Kok, K., Yokota, J., Buys, C. H., Terada, M., & Koeffler, H. P. (1992). p53 mutations in human lung tumors. *Cancer Res*, *52*(7), 1695-1698. https://www.ncbi.nlm.nih.gov/pubmed/1312896

Mok, B. Y., de Moraes, M. H., Zeng, J., Bosch, D. E., Kotrys, A. V., Raguram, A., Hsu, F., Radey, M. C., Peterson, S. B., Mootha, V. K., Mougous, J. D., & Liu, D. R. (2020). A bacterial cytidine deaminase toxin enables CRISPR-free mitochondrial base editing. *Nature*, *583*(7817), 631-637. https://doi.org/10.1038/s41586-020-2477-4

Mueckler, M., Caruso, C., Baldwin, S. A., Panico, M., Blench, I., Morris, H. R., Allard, W. J., Lienhard, G. E., & Lodish, H. F. (1985). Sequence and structure of a human glucose transporter. *Science*, *229*(4717), 941-945. https://doi.org/10.1126/science.3839598

Nguyen, T. P., Fang, M., Kim, J., Wang, B., Lin, E., Khivansara, V., Barrows, N., Rivera-Cancel, G., Goralski, M., Cervantes, C. L., Xie, S., Peterson, J. M., Povedano, J. M., Antczak, M. I., Posner, B. A., Harvey, C. J. B., Naughton, B. T., McFadden, D. G., Ready, J. M., . . . Nijhawan, D. (2023). Inducible mismatch repair streamlines forward genetic approaches to target identification of cytotoxic small molecules. *Cell Chem Biol*, *30*(11), 1453-1467 e1458. https://doi.org/10.1016/j.chembiol.2023.07.017

Nishimura, K., Fukagawa, T., Takisawa, H., Kakimoto, T., & Kanemaki, M. (2009). An auxin-based degron system for the rapid depletion of proteins in nonplant cells. *Nat Methods*, *6*(12), 917-922. https://doi.org/10.1038/nmeth.1401

Nolfi-Donegan, D., Braganza, A., & Shiva, S. (2020). Mitochondrial electron transport chain: Oxidative phosphorylation, oxidant production, and methods of measurement. *Redox Biol*, *37*, 101674. https://doi.org/10.1016/j.redox.2020.101674

Olivier, M., Eeles, R., Hollstein, M., Khan, M. A., Harris, C. C., & Hainaut, P. (2002). The IARC TP53 database: new online mutation analysis and recommendations to users. *Hum Mutat*, *19*(6), 607-614. https://doi.org/10.1002/humu.10081

Parsons, A. B., Brost, R. L., Ding, H., Li, Z., Zhang, C., Sheikh, B., Brown, G. W., Kane, P. M., Hughes, T. R., & Boone, C. (2004). Integration of chemical-genetic and genetic interaction data links bioactive compounds to cellular target pathways. *Nat Biotechnol*, *22*(1), 62-69. https://doi.org/10.1038/nbt919

Petruzzella, V., Vergari, R., Puzziferri, I., Boffoli, D., Lamantea, E., Zeviani, M., & Papa, S. (2001). A nonsense mutation in the NDUFS4 gene encoding the 18 kDa (AQDQ) subunit of complex I abolishes assembly and activity of the complex in a patient with Leigh-like syndrome. *Hum Mol Genet*, *10*(5), 529-535. https://doi.org/10.1093/hmg/10.5.529

Povedano, J. M., Liou, J., Wei, D., Srivatsav, A., Kim, J., Xie, Y., Nijhawan, D., & McFadden, D. G. (2019). Engineering Forward Genetics into Cultured Cancer Cells for Chemical Target Identification. *Cell Chem Biol*, *26*(9), 1315-1321 e1313. https://doi.org/10.1016/j.chembiol.2019.06.006

Ruf, J., & Carayon, P. (2006). Structural and functional aspects of thyroid peroxidase. *Arch Biochem Biophys*, *445*(2), 269-277. https://doi.org/10.1016/j.abb.2005.06.023

Satoh, M., & Kuroiwa, T. (1991). Organization of multiple nucleoids and DNA molecules in mitochondria of a human cell. *Exp Cell Res*, *196*(1), 137-140. https://doi.org/10.1016/0014-4827(91)90467-9

Schaffer, B. E., Park, K. S., Yiu, G., Conklin, J. F., Lin, C., Burkhart, D. L., Karnezis, A. N., Sweet-Cordero, E. A., & Sage, J. (2010). Loss of p130 accelerates tumor development in a mouse model for human small-cell lung carcinoma. *Cancer Res*, *70*(10), 3877-3883. https://doi.org/10.1158/0008-5472.CAN-09-4228

Schmid-Burgk, J. L., Honing, K., Ebert, T. S., & Hornung, V. (2016). CRISPaint allows modular base-specific gene tagging using a ligase-4-dependent mechanism. *Nat Commun*, *7*, 12338. https://doi.org/10.1038/ncomms12338

Sellers, K., Fox, M. P., Bousamra, M., 2nd, Slone, S. P., Higashi, R. M., Miller, D. M., Wang, Y., Yan, J., Yuneva, M. O., Deshpande, R., Lane, A. N., & Fan, T. W. (2015). Pyruvate carboxylase is critical for non-small-cell lung cancer proliferation. *J Clin Invest*, *125*(2), 687-698. https://doi.org/10.1172/JCI72873

Shlien, A., Campbell, B. B., de Borja, R., Alexandrov, L. B., Merico, D., Wedge, D., Van Loo, P., Tarpey, P. S., Coupland, P., Behjati, S., Pollett, A., Lipman, T., Heidari, A., Deshmukh, S., Avitzur, N., Meier, B., Gerstung, M., Hong, Y., Merino, D. M., . . . Biallelic Mismatch Repair Deficiency, C. (2015). Combined hereditary and somatic mutations of replication error repair genes result in rapid onset of ultra-hypermutated cancers. *Nat Genet*, *47*(3), 257-262. https://doi.org/10.1038/ng.3202

Singh, J., Chandra, A., Srilatha, T., Jain, T., Raja, D., & Agrawal, R. (2023). Oncocytoma of the parotid gland: A rare benign tumour. *J Oral Maxillofac Pathol*, *27*(Suppl 1), S41-S44. https://doi.org/10.4103/jomfp.jomfp_437_21

Stroud, D. A., Formosa, L. E., Wijeyeratne, X. W., Nguyen, T. N., & Ryan, M. T. (2013). Gene knockout using transcription activator-like effector nucleases (TALENs) reveals that human NDUFA9 protein is essential for stabilizing the junction between membrane and matrix arms of complex I. *J Biol Chem*, *288*(3), 1685-1690. https://doi.org/10.1074/jbc.C112.436766

Stroud, D. A., Surgenor, E. E., Formosa, L. E., Reljic, B., Frazier, A. E., Dibley, M. G., Osellame, L. D., Stait, T., Beilharz, T. H., Thorburn, D. R., Salim, A., & Ryan, M. T. (2016). Accessory subunits are integral for assembly and function of human mitochondrial complex I. *Nature*, *538*(7623), 123-126. https://doi.org/10.1038/nature19754

Sullivan, L. B., Gui, D. Y., Hosios, A. M., Bush, L. N., Freinkman, E., & Vander Heiden, M. G. (2015). Supporting Aspartate Biosynthesis Is an Essential Function of Respiration in Proliferating Cells. *Cell*, *162*(3), 552-563. https://doi.org/10.1016/j.cell.2015.07.017

Takahashi, T., Takahashi, T., Suzuki, H., Hida, T., Sekido, Y., Ariyoshi, Y., & Ueda, R. (1991). The p53 gene is very frequently mutated in small-cell lung cancer with a distinct nucleotide substitution pattern. *Oncogene*, *6*(10), 1775-1778. https://www.ncbi.nlm.nih.gov/pubmed/1656362

Tallini, G. (1998). Oncocytic tumours. *Virchows Arch*, *433*(1), 5-12. https://doi.org/10.1007/s004280050209

Tallini, G., Ladanyi, M., Rosai, J., & Jhanwar, S. C. (1994). Analysis of nuclear and mitochondrial DNA alterations in thyroid and renal oncocytic tumors. *Cytogenet Cell Genet*, *66*(4), 253-259. https://doi.org/10.1159/000133706

Tran, B., Kopetz, S., Tie, J., Gibbs, P., Jiang, Z. Q., Lieu, C. H., Agarwal, A., Maru, D. M., Sieber, O., & Desai, J. (2011). Impact of BRAF mutation and microsatellite instability on the pattern of metastatic spread and prognosis in metastatic colorectal cancer. *Cancer*, *117*(20), 4623-4632. https://doi.org/10.1002/cncr.26086

Trifunovic, A., Wredenberg, A., Falkenberg, M., Spelbrink, J. N., Rovio, A. T., Bruder, C. E., Bohlooly, Y. M., Gidlof, S., Oldfors, A., Wibom, R., Tornell, J., Jacobs, H. T., & Larsson, N. G. (2004). Premature ageing in mice expressing defective mitochondrial DNA polymerase. *Nature*, *429*(6990), 417-423. https://doi.org/10.1038/nature02517

Tsybrovskyy, O., De Luise, M., de Biase, D., Caporali, L., Fiorini, C., Gasparre, G., Carelli, V., Hackl, D., Imamovic, L., Haim, S., Sobrinho-Simoes, M., & Tallini, G. (2022). Papillary thyroid carcinoma tall cell variant shares accumulation of mitochondria, mitochondrial DNA mutations, and loss of oxidative phosphorylation complex I integrity with oncocytic tumors. *J Pathol Clin Res*, *8*(2), 155-168. https://doi.org/10.1002/cjp2.247

Wacker, S. A., Houghtaling, B. R., Elemento, O., & Kapoor, T. M. (2012). Using transcriptome sequencing to identify mechanisms of drug action and resistance. *Nat Chem Biol*, *8*(3), 235-237. https://doi.org/10.1038/nchembio.779

Wada, N., Duh, Q. Y., Miura, D., Brunaud, L., Wong, M. G., & Clark, O. H. (2002). Chromosomal aberrations by comparative genomic hybridization in hurthle cell thyroid carcinomas are associated with tumor recurrence. *J Clin Endocrinol Metab*, *87*(10), 4595-4601. https://doi.org/10.1210/jc.2002-020339

Wang, G., Shang, L., Burgett, A. W., Harran, P. G., & Wang, X. (2007). Diazonamide toxins reveal an unexpected function for ornithine delta-amino transferase in mitotic cell division. *Proc Natl Acad Sci U S A*, *104*(7), 2068-2073. https://doi.org/10.1073/pnas.0610832104

Wang, T., Wang, J., Hu, X., Huang, X. J., & Chen, G. X. (2020). Current understanding of glucose transporter 4 expression and functional mechanisms. *World J Biol Chem*, *11*(3), 76-98. https://doi.org/10.4331/wjbc.v11.i3.76

Wang, X., Shelton, S. D., Bordieanu, B., Frank, A. R., Yi, Y., Venigalla, S. S. K., Gu, Z., Lenser, N. P., Glogauer, M., Chandel, N. S., Zhao, H., Zhao, Z., McFadden, D. G., & Mishra, P. (2022). Scinderin promotes fusion of electron transport chain dysfunctional muscle stem cells with myofibers. *Nat Aging*, *2*(2), 155-169. https://doi.org/10.1038/s43587-021-00164-x

Warburg, O., Wind, F., & Negelein, E. (1927). The Metabolism of Tumors in the Body. *J Gen Physiol*, *8*(6), 519-530. https://doi.org/10.1085/jgp.8.6.519

Weinberg, F., Hamanaka, R., Wheaton, W. W., Weinberg, S., Joseph, J., Lopez, M., Kalyanaraman, B., Mutlu, G. M., Budinger, G. R., & Chandel, N. S. (2010). Mitochondrial metabolism and ROS generation are essential for Kras-mediated tumorigenicity. *Proc Natl Acad Sci U S A*, *107*(19), 8788-8793. https://doi.org/10.1073/pnas.1003428107

Wiedemann, N., Kozjak, V., Chacinska, A., Schonfisch, B., Rospert, S., Ryan, M. T., Pfanner, N., & Meisinger, C. (2003). Machinery for protein sorting and assembly in the mitochondrial outer membrane. *Nature*, *424*(6948), 565-571. https://doi.org/10.1038/nature01753

Win, A. K., Jenkins, M. A., Dowty, J. G., Antoniou, A. C., Lee, A., Giles, G. G., Buchanan, D. D., Clendenning, M., Rosty, C., Ahnen, D. J., Thibodeau, S. N., Casey, G., Gallinger, S., Le Marchand, L., Haile, R. W., Potter, J. D., Zheng, Y., Lindor, N. M., Newcomb, P. A., . . . MacInnis, R. J. (2017). Prevalence and Penetrance of Major Genes and Polygenes for Colorectal Cancer. *Cancer Epidemiol Biomarkers Prev*, *26*(3), 404-412. https://doi.org/10.1158/1055-9965.EPI-16-0693

Xie, D., Wu, X., Lan, L., Shangguan, F., Lin, X., Chen, F., Xu, S., Zhang, Y., Chen, Z., Huang, K., Wang, R., Wang, L., Song, X., Liu, Y., & Lu, B. (2016). Downregulation of TFAM inhibits the tumorigenesis of non-small cell lung cancer by activating ROS-mediated JNK/p38MAPK signaling and reducing cellular bioenergetics. *Oncotarget*, *7*(10), 11609-11624. https://doi.org/10.18632/oncotarget.7018

Yesbolatova, A., Saito, Y., Kitamoto, N., Makino-Itou, H., Ajima, R., Nakano, R., Nakaoka, H., Fukui, K., Gamo, K., Tominari, Y., Takeuchi, H., Saga, Y., Hayashi, K. I., & Kanemaki, M. T. (2020). The auxin-inducible degron 2 technology provides sharp degradation control in yeast, mammalian cells, and mice. *Nat Commun*, *11*(1), 5701. https://doi.org/10.1038/s41467-020-19532-z

Yuan, Y., Ju, Y. S., Kim, Y., Li, J., Wang, Y., Yoon, C. J., Yang, Y., Martincorena, I., Creighton, C. J., Weinstein, J. N., Xu, Y., Han, L., Kim, H. L., Nakagawa, H., Park, K., Campbell, P. J., Liang, H., & Consortium, P. (2020). Comprehensive molecular characterization of mitochondrial genomes in human cancers. *Nat Genet*, *52*(3), 342-352. https://doi.org/10.1038/s41588-019-0557-x

Yurgelun, M. B., Kulke, M. H., Fuchs, C. S., Allen, B. A., Uno, H., Hornick, J. L., Ukaegbu, C. I., Brais, L. K., McNamara, P. G., Mayer, R. J., Schrag, D., Meyerhardt, J. A., Ng, K., Kidd, J., Singh, N., Hartman, A. R., Wenstrup, R. J., & Syngal, S. (2017). Cancer Susceptibility Gene Mutations in Individuals With Colorectal Cancer. *J Clin Oncol*, *35*(10), 1086-1095. https://doi.org/10.1200/JCO.2016.71.0012

Zhang, T., Dutton-Regester, K., Brown, K. M., & Hayward, N. K. (2016). The genomic landscape of cutaneous melanoma. *Pigment Cell Melanoma Res*, *29*(3), 266-283. https://doi.org/10.1111/pcmr.12459

Zhao, R. Z., Jiang, S., Zhang, L., & Yu, Z. B. (2019). Mitochondrial electron transport chain, ROS generation and uncoupling (Review). *Int J Mol Med*, *44*(1), 3-15. https://doi.org/10.3892/ijmm.2019.4188

Zheng, B., Sage, M., Sheppeard, E. A., Jurecic, V., & Bradley, A. (2000). Engineering mouse chromosomes with Cre-loxP: range, efficiency, and somatic applications. *Mol Cell Biol*, *20*(2), 648-655. https://doi.org/10.1128/MCB.20.2.648-655.2000